AMERICAN SOCIETY FOR MICROBIOLOGY | Molecular and Cellular Biology®

RESEARCH ARTICLE

Nrf2 Suppresses Oxidative Stress and Inflammation in *App* Knock-In Alzheimer's Disease Model Mice

Akira Uruno,[a,b] Daisuke Matsumaru,[c] Rie Ryoke,[d] Ritsumi Saito,[a,b] Shiori Kadoguchi,[b] Daisuke Saigusa,[a,b] Takashi Saito,[e,f] Takaomi C. Saido,[e] Ryuta Kawashima,[d] Masayuki Yamamoto[a,b]

[a]Department of Integrative Genomics, Tohoku Medical Megabank Organization, Tohoku University, Sendai, Miyagi, Japan
[b]Department of Medical Biochemistry, Tohoku University Graduate School of Medicine, Sendai, Miyagi, Japan
[c]Center for Gene Research, Tohoku University, Sendai, Miyagi, Japan
[d]Department of Advanced Brain Science, Institute of Development, Aging and Cancer, Tohoku University, Sendai, Miyagi, Japan
[e]Laboratory for Proteolytic Neuroscience, RIKEN Center for Brain Science, Wako, Saitama, Japan
[f]Department of Neurocognitive Science, Nagoya City University Graduate School of Medical Science, Nagoya, Aichi, Japan

Akira Uruno and Daisuke Matsumaru contributed equally to this article. Author order was determined in order of seniority.

ABSTRACT Nrf2 (NF-E2-related-factor 2) is a stress-responsive transcription factor that protects cells against oxidative stresses. To clarify whether Nrf2 prevents Alzheimer's disease (AD), AD model *App*$^{NL\text{-}G\text{-}F/NL\text{-}G\text{-}F}$ knock-in (*App*^{NLGF}) mice were studied in combination with genetic Nrf2 induction model *Keap1*$^{FA/FA}$ mice. While *App*^{NLGF} mice displayed shorter latency to escape than wild-type mice in the passive-avoidance task, the impairment was improved in *App*^{NLGF}::*Keap1*$^{FA/FA}$ mice. Matrix-assisted laser desorption ionization–mass spectrometry imaging revealed that reduced glutathione levels were elevated by Nrf2 induction in *App*^{NLGF}::*Keap1*$^{FA/FA}$ mouse brains compared to *App*^{NLGF} mouse brains. Genetic Nrf2 induction in *App*^{NLGF} mice markedly suppressed the elevation of the oxidative stress marker 8-OHdG and Iba1-positive microglial cell number. We also determined the plasmalogen-phosphatidylethanolamine (PlsPE) level as an AD biomarker. PlsPE containing polyunsaturated fatty acids was decreased in the *App*^{NLGF} mouse brain, but Nrf2 induction attenuated this decline. To evaluate whether pharmacological induction of Nrf2 elicits beneficial effects for AD treatment, we tested the natural compound 6-MSITC [6-(methylsulfinyl)hexyl isothiocyanate]. Administration of 6-MSITC improved the impaired cognition of *App*^{NLGF} mice in the passive-avoidance task. These results demonstrate that the induction of Nrf2 ameliorates cognitive impairment in the AD model mouse by suppressing oxidative stress and neuroinflammation, suggesting that Nrf2 is an important therapeutic target of AD.

KEYWORDS Nrf2, Alzheimer's disease, oxidative stress, inflammation, glutathione, MALDI-MSI, Alzheimer's disease, Nrf2

The global incidence and prevalence of neurocognitive disorders are increasing worldwide (1). Alzheimer's disease (AD) is one of the most common neurocognitive disorders and is characterized by unique pathological changes, including amyloid β (Aβ) accumulation, plaque formation, hyperphosphorylation of tau protein, and neurofibrillary tangles (NFTs) (2). Oxidative stress and inflammation are increased in the brains of AD patients, and these increases have been widely verified in a number of model animals (3–5). Suppression of the onset and/or progression of AD is an important issue in modern society, and studies have suggested that improvements in these pathological conditions may be beneficial for maintaining or improving the neuronal functions of AD patients.

Our bodies are continuously exposed to various stresses, including reactive

Citation Uruno A, Matsumaru D, Ryoke R, Saito R, Kadoguchi S, Saigusa D, Saito T, Saido TC, Kawashima R, Yamamoto M. 2020. Nrf2 suppresses oxidative stress and inflammation in *App* knock-in Alzheimer's disease model mice. Mol Cell Biol 40:e00467-19. https://doi.org/10.1128/MCB.00467-19.

Address correspondence to Akira Uruno, uruno@med.tohoku.ac.jp, or Masayuki Yamamoto, masiyamamoto@med.tohoku.ac.jp.

Received 29 September 2019
Returned for modification 20 October 2019
Accepted 19 December 2019
Accepted manuscript posted online 13 January 2020
Published 27 February 2020

oxygen/nitrogen species and electrophiles (6), and Nrf2 (NF-E2-related-factor 2) plays critical roles in protecting cells against these stresses (7, 8). Nrf2 is a basic region-leucine zipper-type transcription factor (9) that belongs to the cap'n'collar family (10). In normal unstressed conditions, Keap1 (Kelch-like ECH-associated protein 1) acts as an adaptor for the Cul3-based ubiquitin E3 ligase complex. The E3 ligase efficiently ubiquitinates Nrf2, which brings about rapid Nrf2 degradation through the ubiquitin-proteasome pathway and constitutively suppresses the transcriptional activity of Nrf2 (8, 11). In contrast, when Keap1 is exposed to oxidative and electrophilic stresses, Keap1 cysteine residues are modified, resulting in impairment of the ubiquitin ligase activity of Keap1. Accordingly, Nrf2 degradation is suppressed, and Nrf2 is stabilized and accumulates in the nucleus (11–15). Nrf2 forms a heterodimer with small Maf (sMaf) proteins and binds to the CNC-sMaf-binding element (CsMBE) (16). This stress-responsive transcriptional regulation is called the Keap1-Nrf2 regulatory system (17).

The Keap1-Nrf2 system concomitantly regulates both oxidative stress responses and anti-inflammatory responses. It has been shown that the Keap1-Nrf2 system acts as a key regulator of protective responses against oxidative stresses (17), and Nrf2 induces the expression of many antioxidant enzyme genes (7, 18). An important recent observation is that, in addition to antioxidant enzyme genes, Nrf2 negatively regulates the expression of proinflammatory cytokine genes (19) and modulates the process of inflammation (20). In fact, activation of Nrf2 signaling ameliorates autoimmune disease in mouse models (19, 21–23).

The Keap1-Nrf2 system has been shown to protect neurons in the hypothalamus against oxidative damage (24). A number of studies have also shown that this system plays important roles in the maintenance of brain function (25–28). Indeed, in the brains of AD patients and AD model *App*$^{NL\text{-}G\text{-}F/NL\text{-}G\text{-}F}$ knock-in mice (29), the mRNA and protein expression levels of *NRF2* have been shown to be altered (30, 31). Similarly, glutathione levels and neuroinflammation are shown to be influenced in the brains of mild cognitive impairment and AD patients (32–35). These lines of evidence support the hypothesis that perturbation of the Nrf2-mediated defense system may lead to the pathogenesis of AD. Indeed, *Nrf2* deficiency aggravates the phenotypes of AD model APP/TAU and APP/PS1 mice (36–39), and overexpression of Nrf2 by virus vectors protects hippocampal neurons of APP/PS1 mice and cultured hippocampal cells (40, 41).

Despite these accumulating lines of evidence, however, the roles that Nrf2 plays in AD model animals have not been studied extensively. It remains to be clarified whether Nrf2 induction strongly contributes to protection against AD. To this end, we decided to use *Keap1* knockdown mice, which generally express high levels of Nrf2 in various tissues (42). We refer to this Nrf2 induction as "genetic induction of Nrf2" in contrast to drug-mediated "pharmacological induction of Nrf2." In this study, we exploited *Keap1*$^{floxA/floxA}$ (*Keap1*$^{FA/FA}$) mice as a genetic Nrf2 induction model. We crossed *Keap1*$^{FA/FA}$ mice with *App*$^{NL\text{-}G\text{-}F/NL\text{-}G\text{-}F}$ knock-in mice (referred to as *App*^{NLGF} mice in this study) as an AD model. The *App*^{NLGF} mice harbor the humanized *App* gene with mutations of familial AD, including mutations of Swedish (KM670/671NL), Beyreuther/Iberian (I716F), and Arctic (E693G) (29).

Through analyses of *App*^{NLGF}::*Keap1*$^{FA/FA}$ mice, we found that genetic Nrf2 induction by *Keap1*$^{FA/FA}$ elevated the level of reduced glutathione (GSH) and suppressed oxidative stress and neuroinflammation in the brains of *App*^{NLGF}::*Keap1*$^{FA/FA}$ mice. Genetic Nrf2 induction improved the impaired cognition of *App*^{NLGF}::*Keap1*$^{FA/FA}$ compound mice compared to *App*^{NLGF} mice. We also found that pharmacological Nrf2 induction by a natural compound with mild efficacy and a nonstressful administration route also ameliorated the cognitive impairment of *App*^{NLGF} mice. Thus, this study supports our hypothesis that the induction of Nrf2 in the brain exerts beneficial effects in mice against the development of AD.

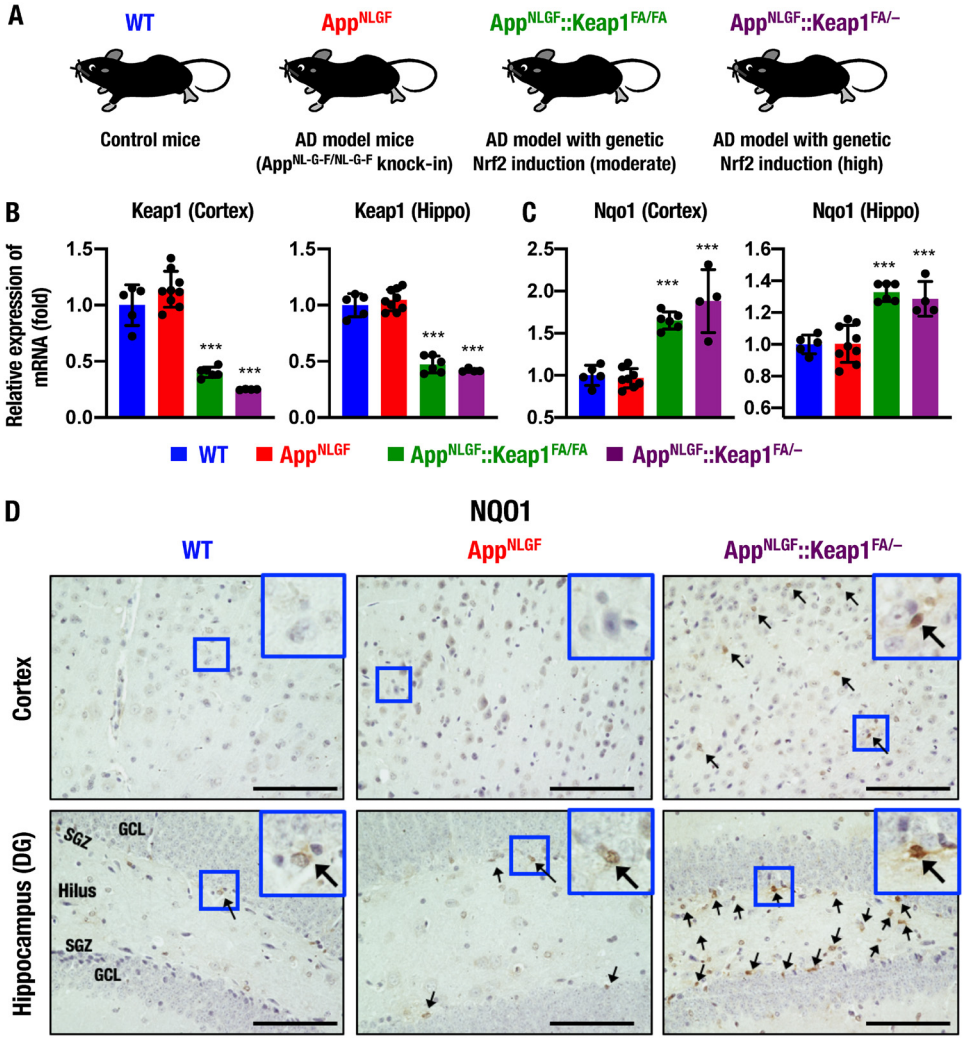

FIG 1 Genetic induction of Nrf2 in AD model *App*^{NLGF} mice. (A) Schematic of WT, *App*^{NLGF}, *App*^{NLGF}::*Keap1*$^{FA/FA}$, and *App*^{NLGF}::*Keap1*$^{FA/-}$ mice. (B and C) Expression levels of *Keap1* (B) and *Nqo1* (C) gene mRNAs in the cerebral cortex and the hippocampus (Hippo), normalized by *Actb* gene expression. The expression levels in WT mice were set to 1, and the results are presented as means ± the SD. ANOVA, followed by the Fisher LSD *post hoc* test, was performed. **, $P < 0.01$; ***, $P < 0.001$ versus *App*^{NLGF} mice. (D) Immunohistochemistry of NQO1 in the cerebral cortex (upper) and the hippocampal dentate gyrus (DG, lower) in WT, *App*^{NLGF}, and *App*^{NLGF}::*Keap1*$^{FA/-}$ mice. Arrows indicate NQO1-positive cells. Scale bars, 100 μm. GCL, granule cell layer; SGZ, subgranular zone.

RESULTS

Genetic Nrf2 induction in AD model mouse brains. To assess whether Nrf2 induction protects AD model mice against disease progression, we crossed *Keap1* knockdown (*Keap1*$^{FA/FA}$) or heterozygous *Keap1* knockout (*Keap1*$^{+/-}$) mice with *App*$^{NL-G-F/NL-G-F}$ (abbreviated here as *App*^{NLGF}) mice to generate *App*^{NLGF}::*Keap1*$^{FA/FA}$ and *App*^{NLGF}::*Keap1*$^{FA/-}$ mice. We expected that these mutant mice would serve as AD models with moderately and highly activated Nrf2 expression, respectively (Fig. 1A). When we evaluated the expression levels of *Keap1* mRNA, we found that the expression levels of *Keap1* in the cerebral cortices and hippocampi of 11-month-old male *App*^{NLGF} mice were comparable with those of age-matched wild-type (WT) male mice. However, *Keap1* expression was decreased to 30 to 50% in the cortices and the hippocampi of *App*^{NLGF}::*Keap1*$^{FA/FA}$ and *App*^{NLGF}::*Keap1*$^{FA/-}$ mice compared with *App*^{NLGF} and WT mice (Fig. 1B).

We also examined expression of the *Nqo1* gene, a representative Nrf2 target gene that exerts an antioxidative response and found that *Nqo1* expression was significantly

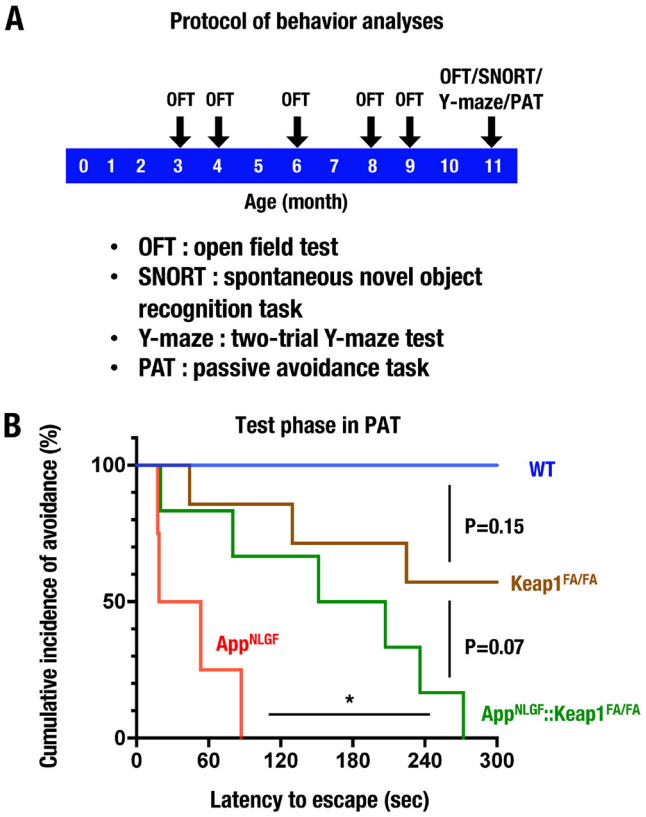

FIG 2 Behavior analyses of *App*^{NLGF} mice. (A) Schematic of the behavior analysis protocol. (B) PAT of 11-month-old male WT ($n = 4$), *Keap1*$^{FA/FA}$ ($n = 7$), *App*^{NLGF} ($n = 4$), and *App*^{NLGF}::*Keap1*$^{FA/FA}$ ($n = 6$) mice. The cumulative incidence of avoidance during the test phase in the PAT is presented as a Kaplan-Meier curve. The log rank test was performed. *, $P < 0.05$.

augmented in both the cortices and the hippocampi of *APP*^{NLGF}::*Keap1*$^{FA/FA}$ and *App*^{NLGF}::*Keap1*$^{FA/-}$ mice (Fig. 1C). These data indicate that the *Keap1*$^{FA/FA}$ and *Keap1*$^{FA/-}$ mutants decrease *Keap1* expression in the brains of *App*^{NLGF} mice, and Nrf2 signaling is indeed activated in *App*^{NLGF}::*Keap1*$^{FA/FA}$ and *App*^{NLGF}::*Keap1*$^{FA/-}$ mouse brains.

To determine cell types in which Nrf2 signaling is activated, immunohistochemical analysis of NQO1 was performed. We could not find NQO1-positive cells in the cortex of WT or *App*^{NLGF} mice; in contrast, NQO1 was expressed in glia-like cells but not in neuron-like cells in the *App*^{NLGF}::*Keap1*$^{FA/-}$ mouse cortex (Fig. 1D, upper). In contrast, several weakly NQO1-positive cells were found in the subgranular zone (SGZ) of the hippocampal dentate gyrus (DG) in WT and *App*^{NLGF} mice, and in *App*^{NLGF}::*Keap1*$^{FA/-}$ mice strongly NQO1-positive cells were detected in the SGZ and the hilus but not in the granule cell layer (GCL) (Fig. 1D, lower). Consistent with previous reports (43, 44), these data suggest that Nrf2 signaling is activated in glial cells but not in neurons in the *App*^{NLGF} mouse brain.

Nrf2 opposes cognitive impairment in *App*^{NLGF} mice. To investigate the roles that Nrf2 plays in the preservation of cognitive functions in *App*^{NLGF} mice, we executed a series of behavioral analyses for WT, *Keap1*$^{FA/FA}$, *App*^{NLGF}, and *App*^{NLGF}::*Keap1*$^{FA/FA}$ mice. As shown in Fig. 2A, mice first performed an open-field test (OFT) at six time points of 3, 4, 6, 8, 9, and 11 months of age. The mice also performed a spontaneous novel object recognition task (SNORT), a two-trial Y-maze test, and a passive-avoidance task (PAT) at 11 months of age.

In 3- to 9-month-old mice, we found no significant differences in the total distance of OFT among the WT, *Keap1*$^{FA/FA}$, *App*^{NLGF}, and *App*^{NLGF}::*Keap1*$^{FA/FA}$ mouse groups (see Fig. S1A in the supplemental material). At 11 months of age, the total distance traveled in the OFT in *App*^{NLGF} mice was slightly higher than that in WT mice, but there were no

statistically significant differences among the four mouse groups (Fig. S1B). We also performed SNORT using appetitive behavior to assess the objective learning and memory abilities of mice. However, the discrimination ratios in the test phase of SNORT were comparable among the WT, *Keap1*$^{FA/FA}$, *App*^{NLGF}, and *App*^{NLGF}::*Keap1*$^{FA/FA}$ mouse groups (data not shown). Similarly, the Y-maze test was used to assess spatial memory, but no obvious change was observed among the four genotype groups (data not shown).

We then conducted PAT to evaluate the associative learning and memory of an aversive condition. Latency to escape of *Keap1*$^{FA/FA}$ mice was slightly shorter than that of WT mice, although there was no statistically significant difference in cumulative incidence of avoidance between WT and *Keap1*$^{FA/FA}$ mice (Fig. 2B). Notably, *App*^{NLGF} mice displayed shorter latency to escape and lower cumulative incidence of avoidance than WT mice in the PAT analysis (Fig. 2B). In contrast, the latency to escape was significantly prolonged in *App*^{NLGF}::*Keap1*$^{FA/FA}$ mice compared to *App*^{NLGF} mice. These results thus demonstrate impaired cognitive functions in *App*^{NLGF} mice. However, genetic Nrf2 induction improves the impaired cognition, especially the decline of emotional associative memory, in the *App*^{NLGF} mice.

Nrf2 suppresses proinflammatory response and phagocytic cells in the *App*^{NLGF} mouse brain. To clarify the molecular basis of how Nrf2 improves the AD phenotype of *App*^{NLGF} mice, we examined whether Nrf2 ameliorates proinflammatory response in the *App*^{NLGF} mouse brain. To this end, we analyzed the expression of proinflammatory cytokine genes in the mouse brains. Although the mRNA levels of proinflammatory cytokine genes *Il6* and *Il1b* were significantly increased in the cerebral cortex and the hippocampus of *App*^{NLGF} mice compared to WT mice (Fig. 3A and B), the expression levels of these genes were reduced in both the cerebral cortex and the hippocampus of *App*^{NLGF}::*Keap1*$^{FA/FA}$ and *App*^{NLGF}::*Keap1*$^{FA/-}$ mice compared to *App*^{NLGF} mice, except for *Il1b* gene expression in the cerebral cortex of *App*^{NLGF}::*Keap1*$^{FA/FA}$ mice. These results suggest that the induction of Nrf2 may ameliorate the AD phenotype of *App*^{NLGF} mice by reducing inflammation in the brain.

We next analyzed the distribution of phagocytic cells in hematoxylin-eosin (HE)-stained sections of the *App*^{NLGF} mouse cortex. We found clusters of phagocytic cells with small and condensed nuclei accumulated around the Aβ depositions in the *App*^{NLGF} mouse cortex (Fig. 3C, middle panel, arrows), which were not observed in the WT mouse cortex (left panel). Notably, the phagocyte-like cells around the Aβ depositions were rarely observed in the brains of *App*^{NLGF}::*Keap1*$^{FA/FA}$ mice (right panel). Although it has been reported that the Nrf2-inducing compounds dimethyl fumarate (DMF) and sulforaphane increase phagocytic activity (45, 46), these data demonstrate that phagocytic cells are suppressed by genetic Nrf2 induction in the brain.

We also performed immunofluorescent staining for the microglial marker ionized calcium-binding adapter molecule 1 (Iba1) (24). Consistent with the results of the HE-stained sections, in the *App*^{NLGF} mouse cortex, Iba1-positive microglia (Fig. 3D, left panel, arrows) were clustered around the amyloid plaques, as shown by the dotted lines. In stark contrast, in *App*^{NLGF}::*Keap1*$^{FA/FA}$ mice, Iba1-positive microglia were not clustered near the amyloid plaques, but Iba1-positive microglia were frequently found at locations not typically associated with amyloid plaques (right panel, yellow arrows). The number of amyloid plaque-associated Iba1-positive microglia in each plaque was significantly decreased in the *App*^{NLGF}::*Keap1*$^{FA/FA}$ mouse cortex compared to the *App*^{NLGF} mouse brain cortex (Fig. 3E). In addition, the number of amyloid plaque-associated Iba1-positive microglia per square millimeter of tissue was also decreased in the cortices of *App*^{NLGF}::*Keap1*$^{FA/FA}$ mice (Fig. 3F).

To further evaluate inflammation in *App*^{NLGF} mouse brain, inflammation mediator genes were examined. *Nos2* mRNA expression was increased in the hippocampi, but not in the cerebral cortices, of *App*^{NLGF} mice compared to WT mice, but the expression levels in the brains of *App*^{NLGF}::*Keap1*$^{FA/FA}$ and *App*^{NLGF}::*Keap1*$^{FA/-}$ mice were comparable to *App*^{NLGF} mice (Fig. S2A). In contrast, *Ptgs2* gene mRNA expression levels were comparable among the four mouse groups (Fig. S2B). These data support the notion

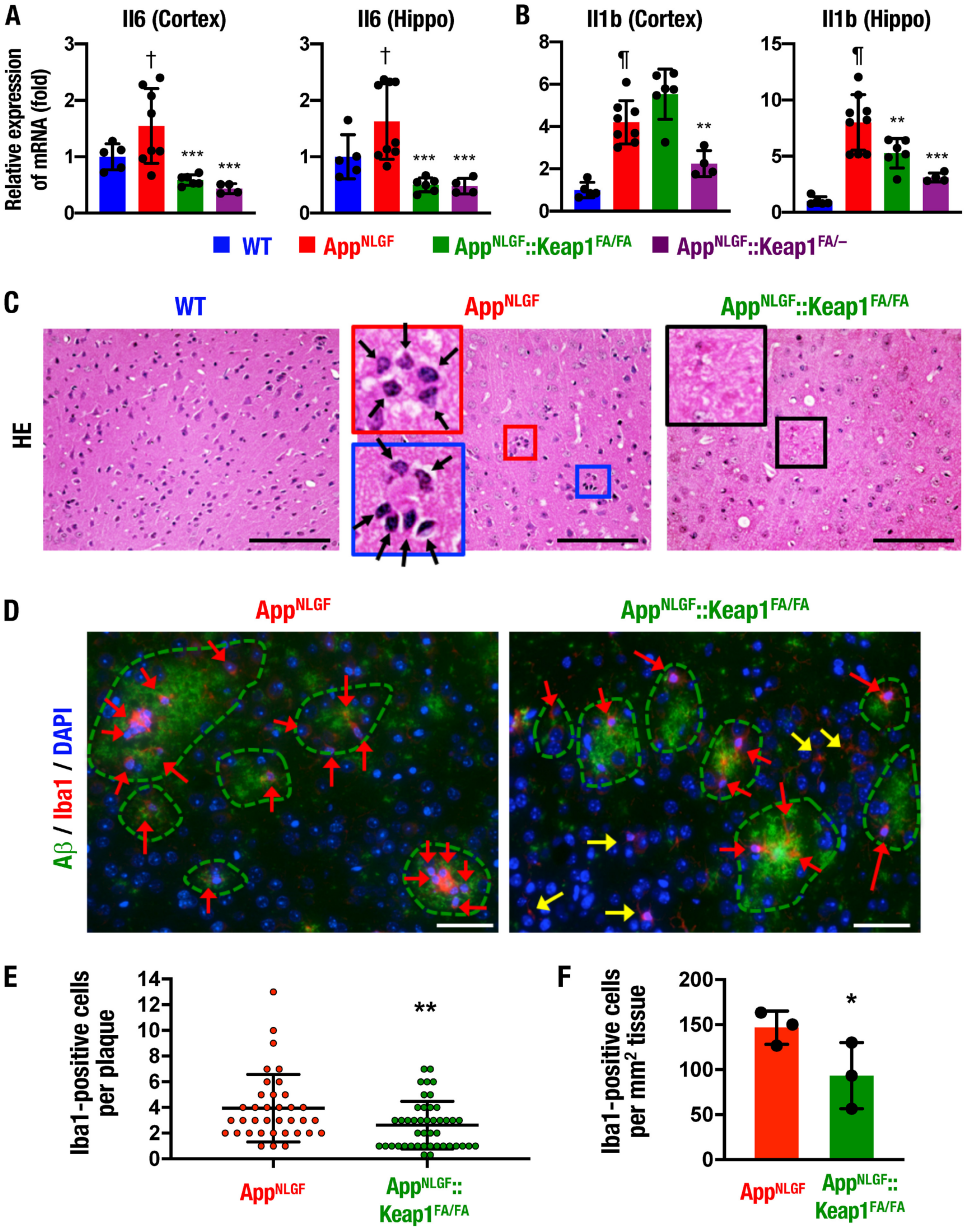

FIG 3 Proinflammatory response and phagocytic cells and Nrf2 expression in the *App*^{NLGF} mouse brain. (A and B) Expression levels of *Il6* (A) and *Il1b* (B) gene mRNAs in the cerebral cortex and the hippocampus (Hippo), normalized by *Actb* gene expression. The expression levels of WT mice were set to 1. (C) HE staining in the cerebral cortices of WT, *App*^{NLGF}, and *App*^{NLGF}::*Keap1*$^{FA/FA}$ mice. Arrows, phagocytic cells. (D) Immunofluorescence staining of Aβ (green) and Iba1 (red) in the *App*^{NLGF} and *App*^{NLGF}::*Keap1*$^{FA/FA}$ mouse cortex. Red and yellow arrows indicate plaque-related and plaque-unrelated Iba1-positive cells, respectively. (E) Numbers of Iba1-positive cells in each amyloid plaque in the cerebral cortex. Thirty-six plaques from three *App*^{NLGF} mouse cortices and 44 plaques from three *App*^{NLGF}::*Keap1*$^{FA/FA}$ mouse cortices were counted. (F) Numbers of Iba1-positive cells associated with amyloid plaque per tissue area (square millimeter) in the cerebral cortex. The averages of the numbers in each mouse were calculated in three *App*^{NLGF} and three *App*^{NLGF}::*Keap1*$^{FA/FA}$ mice. The results are presented as means ± the SD. Statistical analyses were performed using ANOVA, followed by Fisher LSD *post hoc* test (A and B) or Student *t* test (E and F). †, $P < 0.05$; ¶, $P < 0.001$ versus WT mice. *, $P < 0.05$; **, $P < 0.01$; ***, $P < 0.001$ versus *App*^{NLGF} mice. Scale bars: 100 μm (C) and 50 μm (D).

that genetic Nrf2 induction suppresses the proinflammatory response and phagocytic cells in the *App*^{NLGF} mouse brain.

Nrf2 suppresses transition of homeostatic microglia to disease-associated microglia. *App*^{NLGF}::*Keap1*$^{FA/FA}$ mice displayed a reduction in Iba1-positive cells associated with amyloid plaques. We then focused on the role of Nrf2 in microglia regulation. We

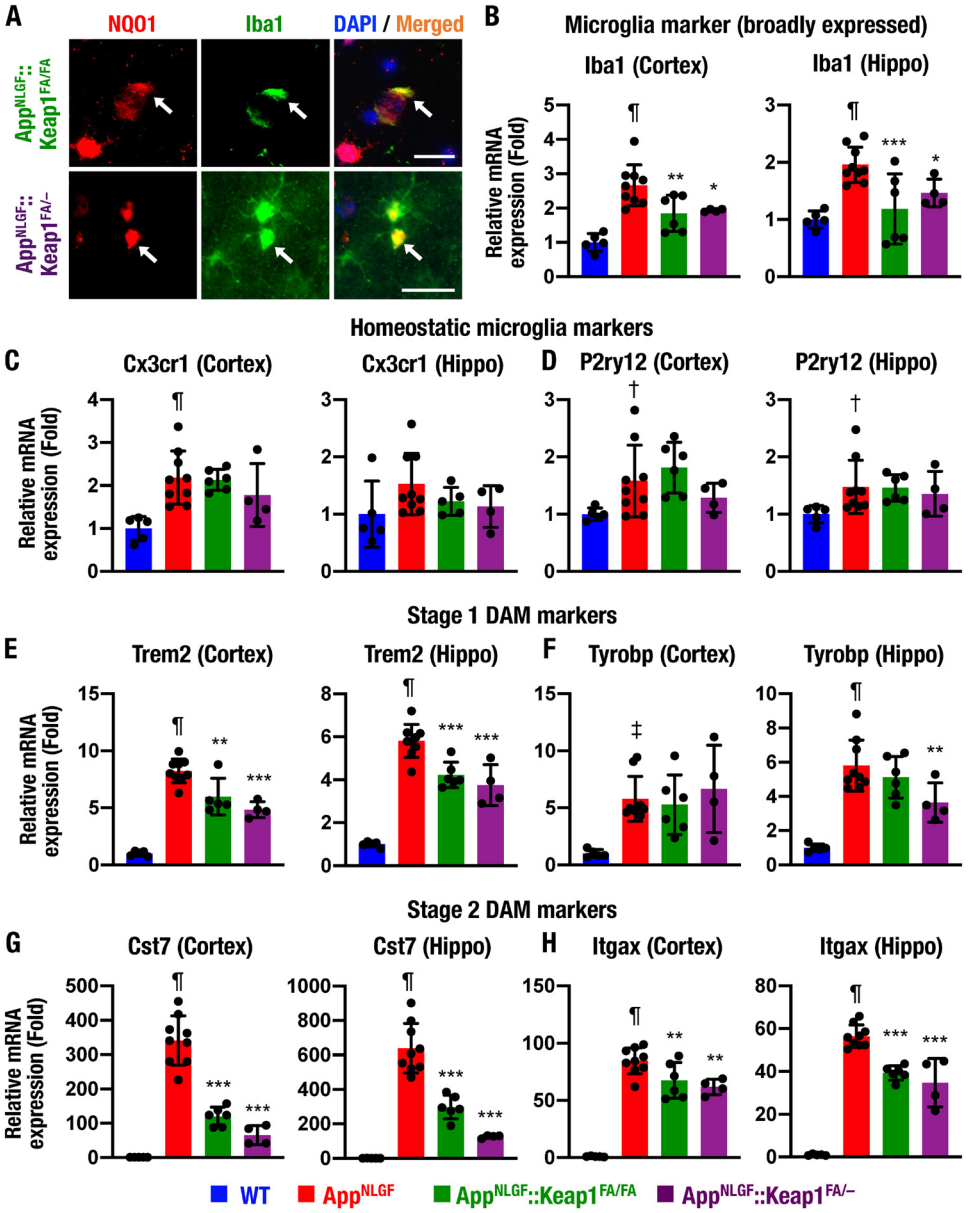

FIG 4 Nrf2 suppresses transition of homeostatic microglia to DAM. (A) Immunofluorescence analysis of NQO1 and Iba1 in the hippocampi of *App*^{NLGF}::*Keap1*$^{FA/FA}$ and *App*^{NLGF}::*Keap1*$^{FA/–}$ mice. Arrows indicate NQO1-positive cells. (B to H) Expression levels of microglia subtype marker gene mRNAs, including a broadly expressed microglia marker *Iba1* (B), homeostatic microglia markers *Cx3cr1* and *P2ry12* (C and D), stage 1 DAM markers *Trem2* and *Tyrobp* (E and F), and stage 2 DAM markers *Cst7* and *Itgax* (G and H), in the cerebral cortex and the hippocampus (Hippo), normalized by *Actb* gene expression. The expression levels in WT mice were set to 1 and are presented as means ± the SD. Statistical analyses were performed using ANOVA, followed by the Fisher LSD *post hoc* test. †, $P < 0.05$; ‡, $P < 0.01$; ¶, $P < 0.001$ versus WT mice. *, $P < 0.05$; **, $P < 0.01$; ***, $P < 0.001$ versus *App*^{NLGF} mice.

examined NQO1 and Iba1 immunostaining and found that the Iba1-positive cells expressed NQO1 in *App*^{NLGF}::*Keap1*$^{FA/FA}$ and *App*^{NLGF}::*Keap1*$^{FA/–}$ mouse brains (Fig. 4A, arrows), indicating that Nrf2 signaling is activated in microglia.

We also examined the expression levels of *Iba1* mRNA in the cortices and the hippocampi of WT, *App*^{NLGF}, *App*^{NLGF}::*Keap1*$^{FA/FA}$, and *App*^{NLGF}::*Keap1*$^{FA/–}$ mouse brains. The *Iba1* mRNA expression levels were markedly increased in both the cortices and the hippocampi of *App*^{NLGF} mice compared to WT mice (Fig. 4B). Importantly, showing very good agreement with the results of histological and immunofluorescent analyses, the induction of *Iba1* mRNA in the *App*^{NLGF} mouse brain was suppressed in both the

cortices and the hippocampi of *App*^{NLGF}::*Keap1*$^{FA/FA}$ and *App*^{NLGF}::*Keap1*$^{FA/-}$ mouse brains.

It has been reported that there are subtypes of microglia (47), including phagocytic and activated subtypes, named disease-associated microglia (DAM) (48–50). Since the phagocytic cells surrounding amyloid plaques were suppressed in *App*^{NLGF}::*Keap1*$^{FA/FA}$ mouse brain, we evaluated whether Nrf2 influences the transition of homeostatic microglia to DAM by examining homeostatic and disease-associated microglial markers.

Homeostatic microglial marker *Cx3cr1* and *P2ry12* gene expression levels were slightly elevated in the cortex and hippocampus of *App*^{NLGF} mice (Fig. 4C and D). However, these expression levels were not suppressed in the cortices or hippocampi of *App*^{NLGF}::*Keap1*$^{FA/FA}$ and *App*^{NLGF}::*Keap1*$^{FA/-}$ mice compared to *App*^{NLGF} mice.

When microglia are activated to exert phagocytic efficacy, they are initially activated to an intermediate subtype, named stage 1 DAM, which increases *Trem2* and *Tyrobp* expression levels (48). The expression of the *Trem2* gene, a stage 1 DAM marker, was markedly increased in *App*^{NLGF} mouse cortex and hippocampus compared to WT mice but was suppressed in *App*^{NLGF}::*Keap1*$^{FA/FA}$ and *App*^{NLGF}::*Keap1*$^{FA/-}$ mouse cortices and hippocampi (Fig. 4E). *Tyrobp* gene expression was also increased in *App*^{NLGF} mouse cortices and hippocampi and repressed in the hippocampi of *App*^{NLGF}::*Keap1*$^{FA/-}$ mice (Fig. 4F).

The stage 1 DAM subtype is activated to stage 2 DAM, which induces the expression of phagocytic cell-related *Cst7* and *Itgax* genes (48). The gene expression levels of the stage 2 DAM markers *Cst7* and *Itgax* were strongly induced in the cortices and hippocampi of *App*^{NLGF} mice, and their inductions were markedly repressed in *App*^{NLGF}::*Keap1*$^{FA/FA}$ and *App*^{NLGF}::*Keap1*$^{FA/-}$ mouse cortices and hippocampi (Fig. 4G and H). These data support the notion that genetic Nrf2 induction suppresses the transition of homeostatic microglia to DAM in the *App*^{NLGF} mouse brain.

Nrf2 attenuates reactive astrocytosis in the *App*^{NLGF} mouse brain. It is known that reactive astrocytosis is a pathological reaction of astrocytes frequently observed in inflammation, and a hallmark of the condition is increased glial fibrillary acidic protein (GFAP)-positive astrocytes (5). NQO1 and GFAP immunostaining revealed that the GFAP-positive cells indeed expressed NQO1 in the *App*^{NLGF}::*Keap1*$^{FA/FA}$ mouse brain (Fig. 5A, arrows).

It has been reported that GFAP-positive astrocytes are increased in the *App*^{NLGF} mouse brain (29). Consistent with this observation, we found that *Gfap* mRNA expression levels were significantly elevated in both the cortices and the hippocampi of *App*^{NLGF} mice compared to WT mice (Fig. 5B). *Gfap* mRNA induction was significantly and moderately suppressed in the cortex of *App*^{NLGF}::*Keap1*$^{FA/-}$ mice and *App*^{NLGF}::*Keap1*$^{FA/FA}$ mice, respectively (left panel). In the hippocampus, these changes in *Gfap* mRNA expression were marginal (right panel).

We also conducted immunofluorescence staining for GFAP, Iba1, and Aβ and found that GFAP-positive cells were broadly increased in the cerebral cortices of *App*^{NLGF} mice but were highly induced around the Aβ-deposited area (Fig. 5C, middle panels, dotted lines) compared to WT mice (left panels). In contrast, a limited number of Iba1-positive cells were expressed around Aβ depositions in the *App*^{NLGF} mouse cortex (middle panels) compared to the WT mouse cortex (left panels). GFAP-positive cells were observed around the Aβ-deposited area, but fewer were found in the cortex of *App*^{NLGF}::*Keap1*$^{FA/FA}$ mice (right panels, dotted lines) than in the cortices of *App*^{NLGF} mice. The quantified GFAP-positive area was higher in the cortices of *App*^{NLGF} mice than in WT mice (Fig. 5D). Although low-level GFAP-stained areas were observed in the *App*^{NLGF}::*Keap1*$^{FA/FA}$ mouse cortex, there was no statistically significant difference between *App*^{NLGF} and *App*^{NLGF}::*Keap1*$^{FA/FA}$ mice. Taken together, these results indicate that genetic Nrf2 induction by *Keap1* gene knockdown partially ameliorates reactive astrocytosis in the *App*^{NLGF} mouse cortex.

Nrf2 inhibits neuronal damage around amyloid plaques. It has been reported that synaptic alterations around amyloid plaques were observed in the brains of

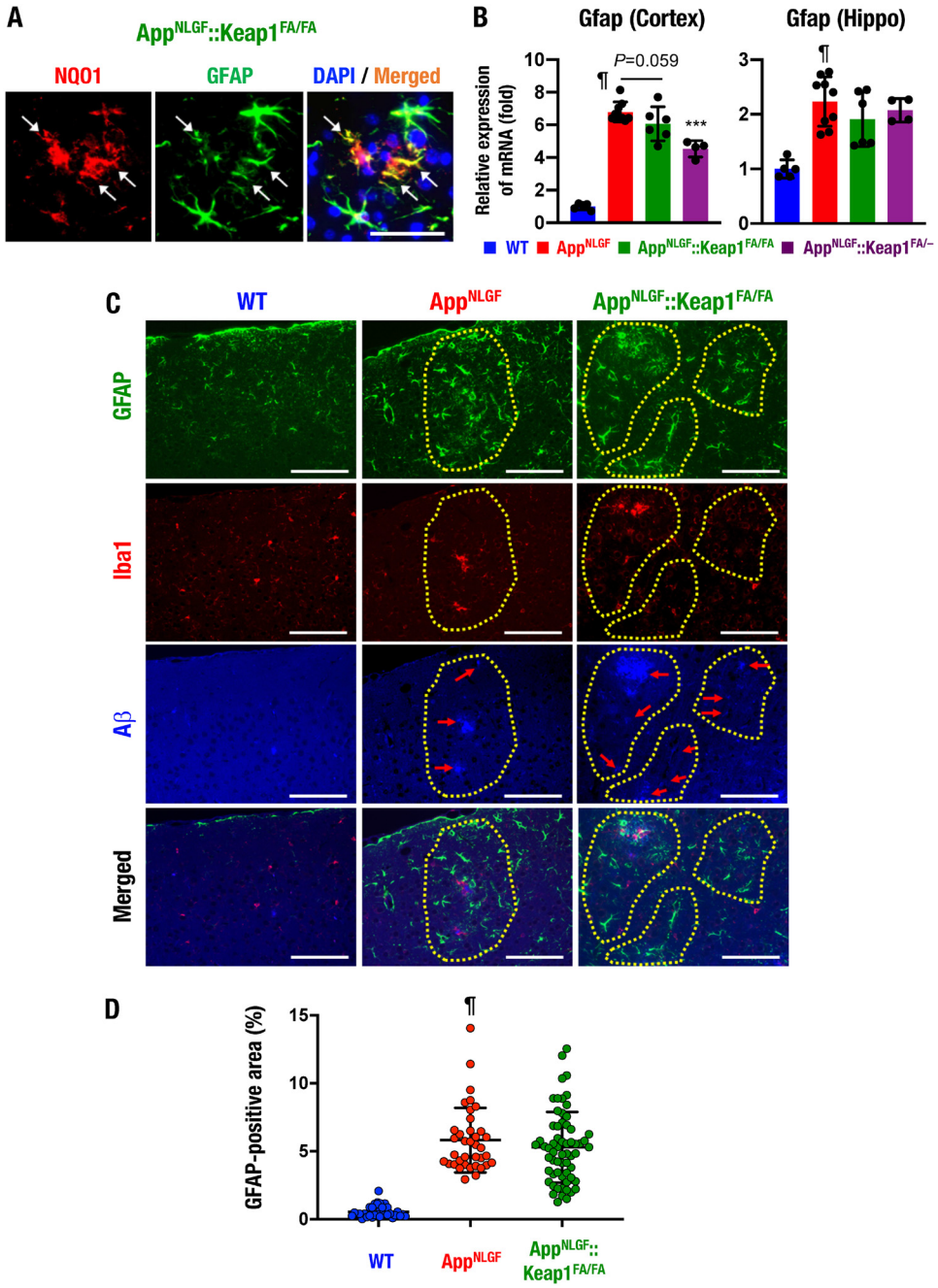

FIG 5 Nrf2 induction ameliorates reactive astrocytosis in the *App*^{NLGF} mouse brain. (A) Immunofluorescence analysis of NQO1 and GFAP in the cerebral cortices of *App*^{NLGF}::*Keap1*$^{FA/FA}$ mice. Arrows indicate NQO1-positive cells. (B) Expression of *Gfap* mRNA in the cerebral cortex and the hippocampus (Hippo), normalized by *Actb* gene expression. The expression levels of WT mice were set to 1. (C) Immunofluorescence analysis of GFAP (green), Iba1 (red), and Aβ (blue) in the cerebral cortices of WT, *App*^{NLGF}, and *App*^{NLGF}::*Keap1*$^{FA/FA}$ mice. Dotted lines indicate Aβ deposit-related areas. (D) GFAP-positive area in the brain cortex. We analyzed 33, 37, and 62 images from three WT, three *App*^{NLGF}, and two *App*^{NLGF}::*Keap1*$^{FA/FA}$ mouse cortices. The results were calculated as the percentage of tissue area and are presented as means $\pm$ the SD. Statistical analyses were performed using ANOVA followed by Fisher LSD *post hoc* test (B) or the Kruskal-Wallis test (D). ¶, $P < 0.001$ versus WT mice. ***, $P < 0.001$ versus *App*^{NLGF} mice. Scale bars: 50 μm (A) and 100 μm (C).

App^{NLGF} mice and AD patients (29). We performed immunostaining of the neuron fiber marker Tuj1 and found that Tuj1-positive staining cells were decreased around amyloid plaques in the cortices of *App*^{NLGF} mice compared to WT mice (Fig. 6A, top and middle, arrows). Importantly, in the *App*^{NLGF}::*Keap1*$^{FA/FA}$ mouse brain, Tuj1 strongly positive neurons were found around plaques (Fig. 6A, bottom, arrows).

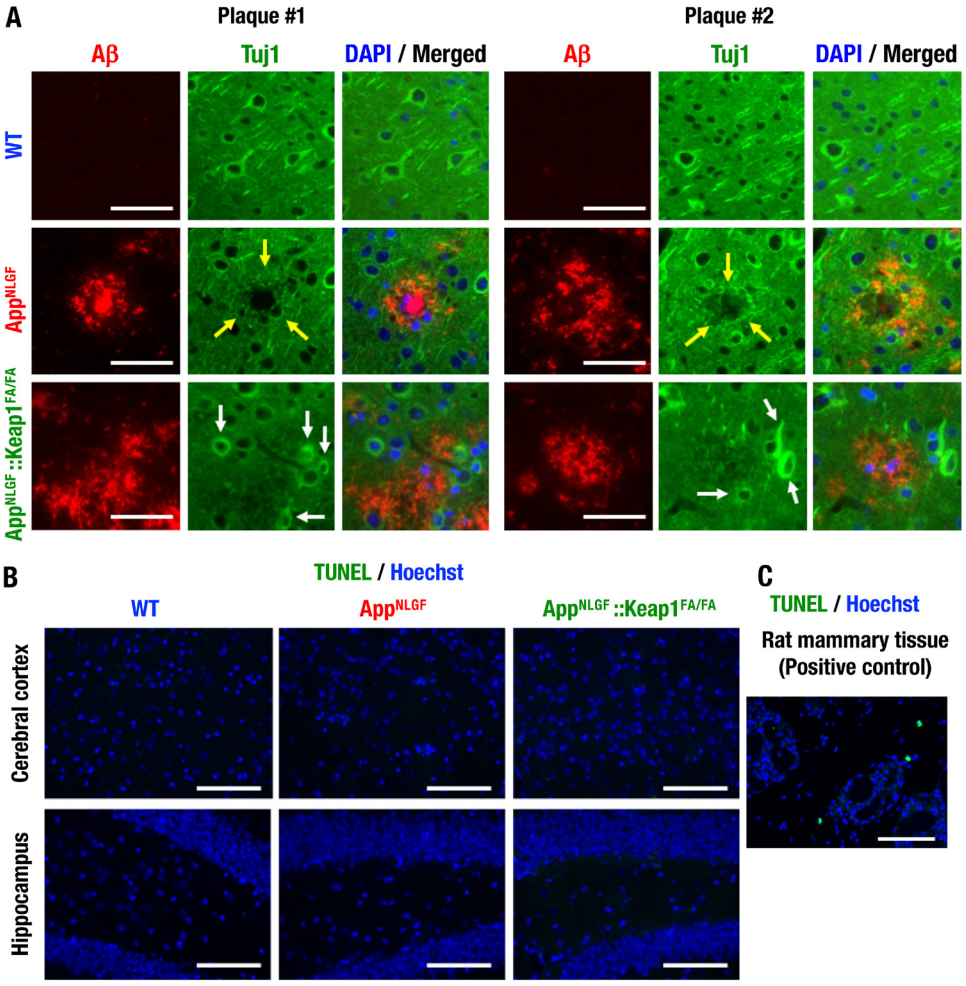

FIG 6 Nrf2 inhibits neuron damage around amyloid plaques. (A) Immunofluorescence analysis of Tuj1 and Aβ in the cerebral cortices of 11-month-old mice. Yellow arrows indicate the decreased Tuj1-positive staining around amyloid plaques. White arrows indicate retained neurons. (B and C) TUNEL assay and Hoechst 33342 straining in the cerebral cortices and the hippocampi of 11-month-old mouse brains (B), with rat mammary tissue as a positive control (C). Scale bars: 50 μm (A) and 100 μm (B and C).

To detect neuronal apoptosis in the brains of *App*^{NLGF} mice, *in situ* detection of fragmented DNA by terminal deoxynucleotidyl-transferase dUTP nick-end labeling (TUNEL) analysis was next performed. The TUNEL-positive cells were not found in the cerebral cortices or hippocampi of WT, *App*^{NLGF}, and *App*^{NLGF}::*Keap1*$^{FA/FA}$ mice (Fig. 6B). In contrast, TUNEL-positive cells were found in rat mammalian tissue as a positive control (Fig. 6C). These data indicate that Nrf2 induction inhibits the decrease in neuronal damage around amyloid plaques independent of apoptosis.

Oxidative stress accumulation in the *App*^{NLGF} mouse brain. To assess oxidative stress levels in the *App*^{NLGF} mouse brain, we conducted an immunohistochemical analysis of the oxidative stress marker 8-hydroxy-2′-deoxyguanosine (8-OHdG) in the brains of WT, *App*^{NLGF}, and *App*^{NLGF}::*Keap1*$^{FA/FA}$ mice. We captured high-magnification images of the regions shown in the low-magnification images in Fig. 7A of the cortex (black boxes), the hippocampal CA1 region (orange boxes), and the DG (green boxes).

Importantly, large numbers of 8-OHdG-positive cells were found in the cortices, the hippocampal CA1 regions, and the DGs of *App*^{NLGF} mice (Fig. 7B and C, middle panels), but essentially no such cells were found in the WT mouse brain (left panels). Importantly, 8-OHdG-positive cells were markedly decreased in the respective regions of the *App*^{NLGF}::*Keap1*$^{FA/FA}$ mouse brain (right panels). A quantifiable number of 8-OHdG-positive cells were induced in the cerebral cortices of *App*^{NLGF} mice compared to WT

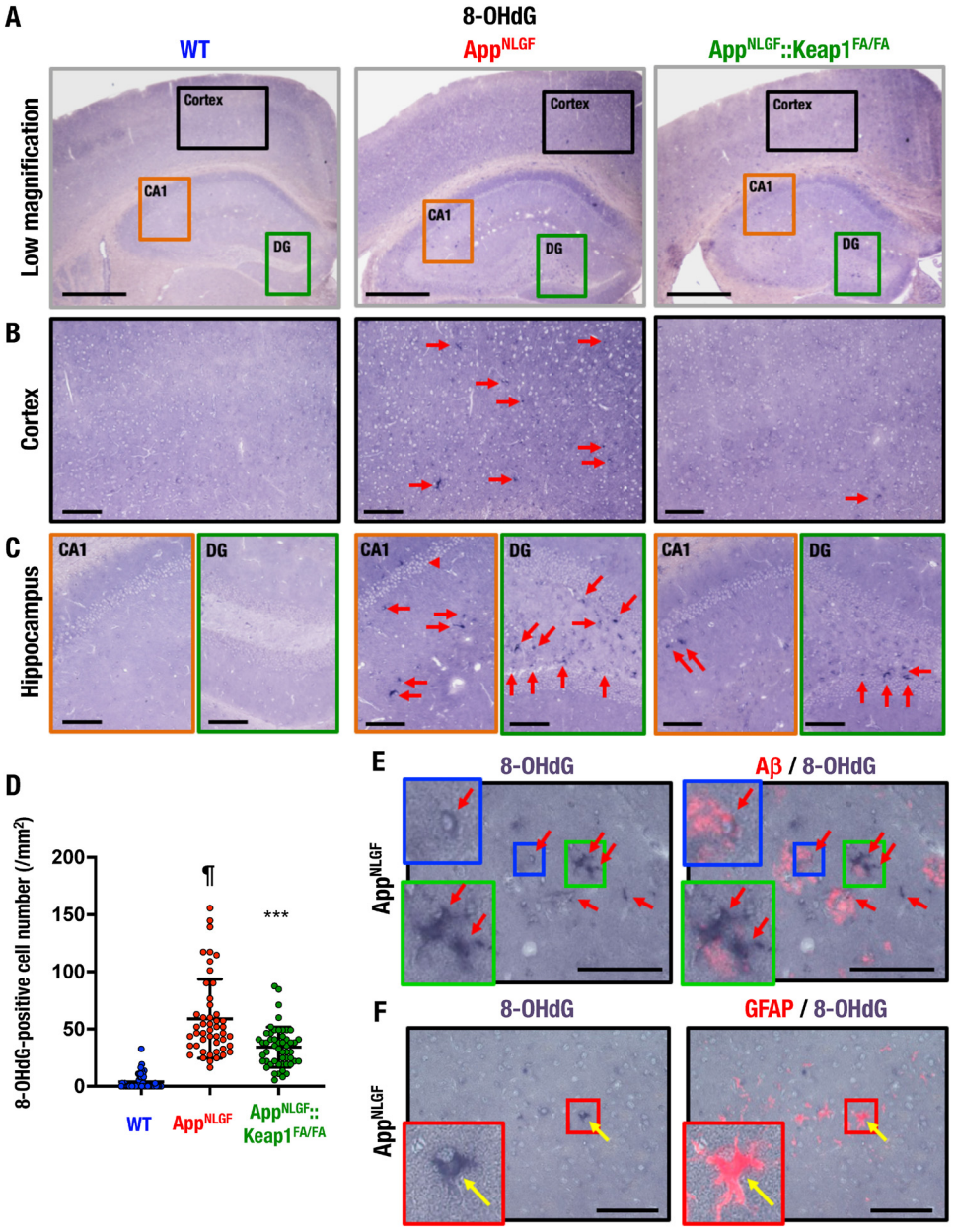

FIG 7 Oxidative stress accumulation in the *App*^{NLGF} mouse brain. (A to C) Immunohistochemistry of the oxidative stress marker 8-OHdG. Shown are low-magnification images acquired using a 4× objective (A) and high-magnification images acquired using a 20× objective of the cerebral cortex (B), the hippocampal CA1 (C, left), and the DG (C, right). (D) Number of 8-OHdG-positive cells in the cortex. We analyzed 48, 48, and 52 images from three each WT, *App*^{NLGF}, and *App*^{NLGF}::*Keap1*$^{FA/FA}$ mouse cortex. The results are presented as the number per square millimeter of tissue and as means ± the SD. Statistical analyses were performed using ANOVA, followed by the Fisher LSD *post hoc* test. ¶, $P < 0.001$ versus WT mice. ***, $P < 0.001$ versus *App*^{NLGF} mice. (E and F) Immunostaining of 8-OHdG and Aβ (E) or GFAP (F) in *App*^{NLGF} mouse cerebral cortex. Arrows indicate 8-OHdG-positive cells. Scale bars: 500 μm (A) and 100 μm (B, C, E, and F).

mice, and the number was decreased in the cortices of *App*^{NLGF}::*Keap1*$^{FA/FA}$ mice compared to *App*^{NLGF} mice (Fig. 7D). Double immunostaining for 8-OHdG and Aβ revealed that the 8-OHdG-positive cells were found around Aβ-stained areas in the *App*^{NLGF} mouse cortex (Fig. 7E, arrows). The 8-OHdG staining was detected in astrocyte-like (Fig. 7E, green boxes) and microglia-like (blue boxes) cells. We also found 8-OHdG- and GFAP-double-stained cells in the cerebral cortices of *App*^{NLGF} mice (Fig. 7F). These results indicate that genetic Nrf2 induction suppresses oxidative stress and 8-OHdG formation in the *App*^{NLGF} mouse brain.

Nrf2 increases GSH levels in the *App*^{NLGF} mouse brain. To clarify how Nrf2 protects the *App*^{NLGF} mouse brain against oxidative tissue damage, we conducted a series of experiments that assessed changes in the antioxidative stress activity of the brain. Nrf2 has been shown to regulate the expression of glutathione synthesis-related enzyme genes (6); therefore, we analyzed the expression levels of *Gclm*, *Gclc*, and *Gsr* genes encoding glutamate-cysteine ligase modifier and catalytic subunits and glutathione reductase, respectively. The expression of *Gclm* mRNA in the cerebral cortex was comparable between WT and *App*^{NLGF} mice, but the mRNA expression level was increased significantly in *App*^{NLGF}::*Keap1*$^{FA/FA}$ and *App*^{NLGF}::*Keap1*$^{FA/-}$ mice compared to *App*^{NLGF} mice (Fig. 8A). In contrast, the expression of *Gclc* mRNA in the cerebral cortex was comparable among these four mouse groups (Fig. 8B). *Gsr* mRNA expression in the cerebral cortex was increased in *App*^{NLGF}::*Keap1*$^{FA/FA}$ mice compared to *App*^{NLGF} mice (Fig. 8C).

We next sought to evaluate GSH levels in the mouse brain *in situ* by means of matrix-assisted laser desorption ionization–mass spectrometry imaging (MALDI-MSI). However, since GSH is highly reactive and easily generates oxidized glutathione (GSSG) (51, 52), we realized the necessity to avoid nonspecific reactions to the thiol residue of GSH. Therefore, we decided to generate GSSG by utilizing *N*-ethylmaleimide (NEM), since NEM has been used for this purpose in liquid chromatography-mass spectrometry (LC-MS) analysis (53). Thus, we applied a challenge application of NEM in MALDI-MSI in this analysis. In the presence of NEM, the cysteine residue of GSH forms a conjugate with NEM and generates GSH-NEM (Fig. 8D), and the tandem mass spectrometry (MS/MS) signal of GSH-NEM should be detected as *m/z* 304 by LC-MS (53). In the MALDI-MSI analysis, the MS/MS signal of GSH-NEM was also detected as *m/z* 304 in brain sections (Fig. 8E), indicating that the NEM method is applicable for MALDI-MSI analysis.

MALDI-MSI analysis coupled with the NEM modification method was used to evaluate the distribution of GSH-NEM signals in brain coronal sections of WT mice at 1.8 mm posterior to the bregma. GSH-NEM signals were detected in the inner cortex, the hippocampus, the hypothalamus, and the thalamus, whereas signals were rarely detected in the outer cortex (Fig. 8F, left panels). GSH-NEM signals were lower in the hippocampi, thalami, and hypothalami of *App*^{NLGF} mice than in those regions of WT mice (middle panels), but these signals were significantly and broadly elevated in the *App*^{NLGF}::*Keap1*$^{FA/FA}$ mouse brain (right panels). These results thus demonstrate that GSH levels in various parts of the brain are increased in the *App*^{NLGF}::*Keap1*$^{FA/FA}$ mouse brain, perhaps due to the increased Nrf2 activity.

Nrf2 induction does not significantly change Aβ deposition. We next examined Aβ accumulation in the brains of WT, *App*^{NLGF}, *App*^{NLGF}::*Keap1*$^{FA/FA}$, and *App*^{NLGF}::*Keap1*$^{FA/-}$ mice by means of immunohistochemistry. Consistent with the previous report that Aβ accumulated in the brains of *App*^{NLGF} mice from 2 to 7 months of age (29), we found in this study that Aβ was highly deposited in 11-month-old *App*^{NLGF} mouse brains. Aβ depositions in *App*^{NLGF}::*Keap1*$^{FA/FA}$ and *App*^{NLGF}::*Keap1*$^{FA/-}$ mice were comparable with those of *App*^{NLGF} mice, as shown by the low-magnification images in Fig. 9A.

Inspection of higher-magnification images of the cortex (Fig. 9B) and the hippocampus (Fig. 9C) further verified that Aβ deposition levels in *App*^{NLGF}::*Keap1*$^{FA/FA}$ and *App*^{NLGF}::*Keap1*$^{FA/-}$ mice were comparable with that in *App*^{NLGF} mice. To determine the Aβ accumulation, we also performed immunofluorescent staining and enzyme-linked immunosorbent assay (ELISA) of Aβ in the *App*^{NLGF} mouse brain. The immunofluorescent staining of Aβ revealed that the percentages of the Aβ-positive area in the cortex were comparable between *App*^{NLGF} and *App*^{NLGF}::*Keap1*$^{FA/FA}$ mice (Fig. 9D and E). The ELISA showed that the soluble Aβ(1-40) (F) and Aβ(1-42) levels were comparable among cerebral cortices and hippocampi in *App*^{NLGF} and *App*^{NLGF}::*Keap1*$^{FA/FA}$ mouse brains (Fig. 9F and G). These results demonstrate that the genetic induction of Nrf2

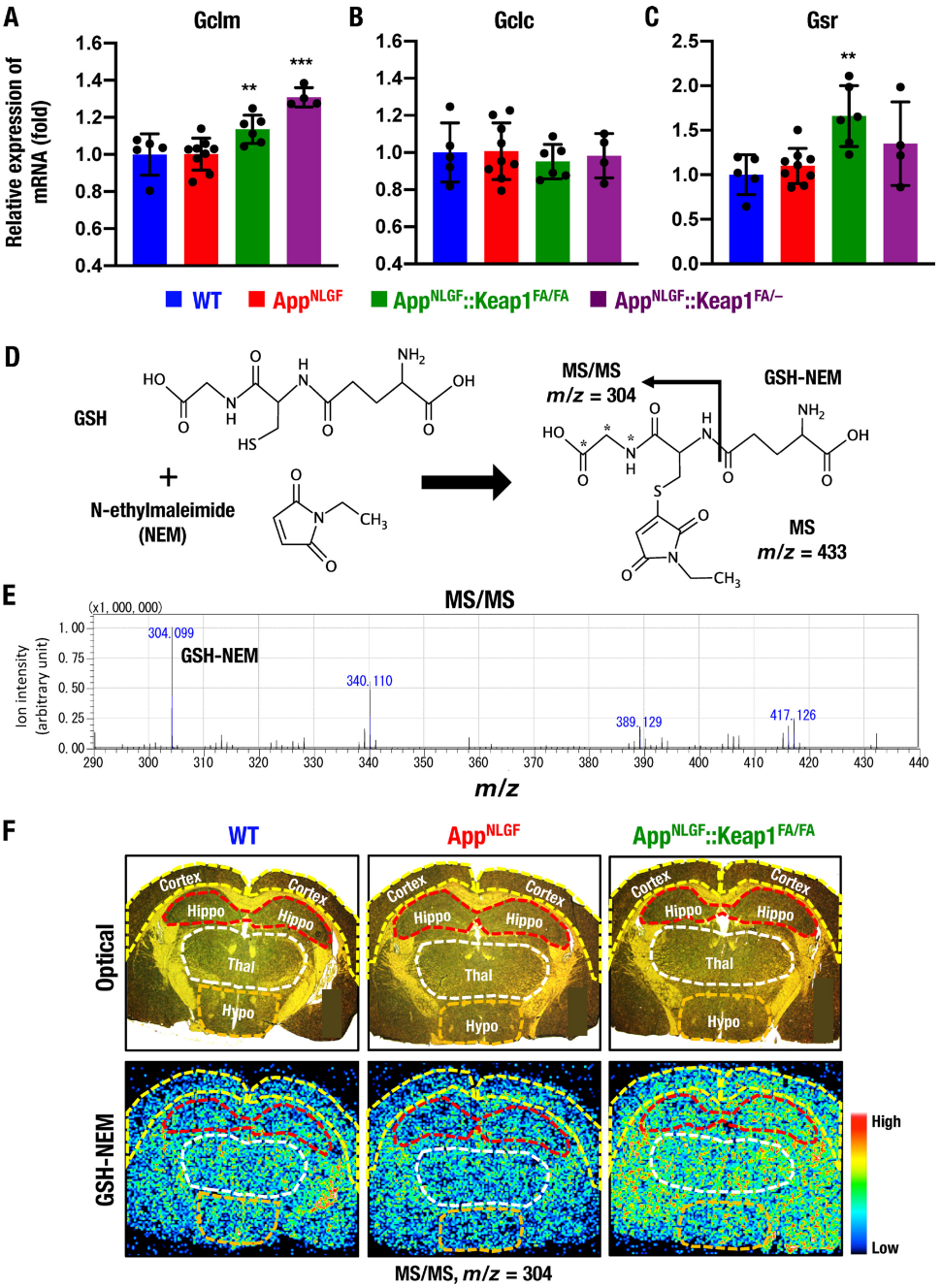

FIG 8 Nrf2 increases GSH levels in *App*^{NLGF}::*Keap1*$^{FA/FA}$ mouse brains. (A to C) Expression levels of glutathione-related *Gclm* (A), *Gclc* (B), and *Gsr* (C) genes in the cerebral cortex, normalized by *Actb* gene expression. The expression levels in WT mice were set to 1, and the results are presented as means ± the SD. Note that the *Gclm* expression levels were significantly elevated in *App*^{NLGF} and *App*^{NLGF}::*Keap1*$^{FA/FA}$ mouse brains. Statistical analyses were performed using ANOVA, followed by the Fisher LSD *post hoc* test. **, $P < 0.01$; ***, $P < 0.001$ versus *App*^{NLGF} mice. (D to F) MALDI-MSI analysis of GSH in the brain. (D) In the presence of NEM, the thiol residue of GSH conjugates with NEM, and MS/MS signals of GHS-NEM were calculated to be detected as *m/z* 304. (E) MS/MS signals of GHS-NEM from NEM-treated brain sections were detected as *m/z* 304.099 by MALDI-MSI analysis. (F) Optical (upper) and MS/MS (lower) images of GHS-NEM signals (*m/z* 304) in brain sections of 11-month-old male WT, *App*^{NLGF} and *App*^{NLGF}::*Keap1*$^{FA/FA}$ mice at positions 8 mm posterior to the bregma. Cortex, cerebral cortex (yellow lines); Hippo, hippocampus (red lines); Thal, thalamus (white line); Hypo, hypothalamus (orange lines).

ameliorates oxidative tissue damage and proinflammatory response in the *App*^{NLGF} mouse brain without significantly changing Aβ deposition.

6-MSITC prevents cognitive impairment in *App*^{NLGF} mice by inducing Nrf2. A natural compound, 6-(methylsulfinyl)hexyl isothiocyanate (6-MSITC), which is contained

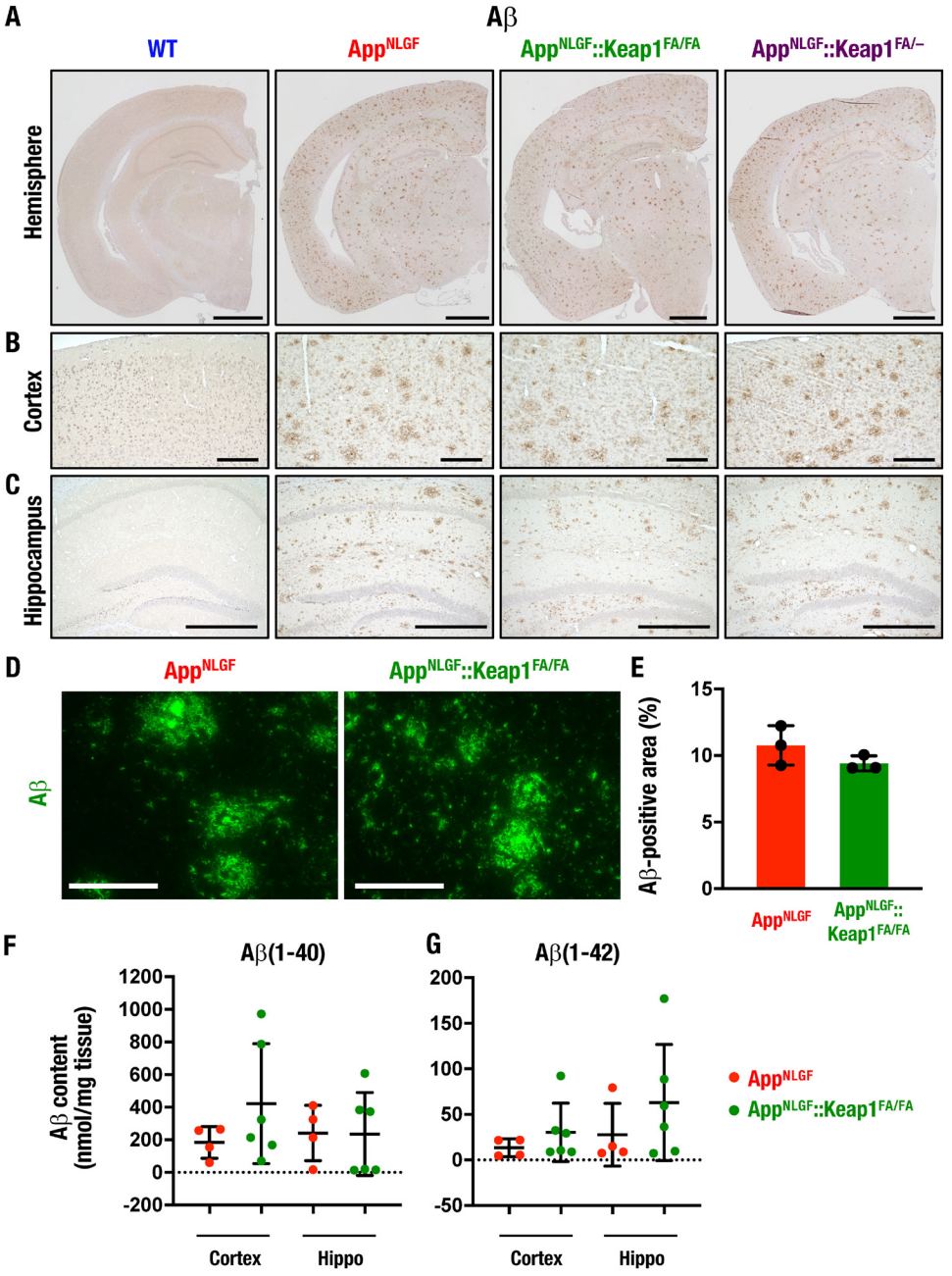

FIG 9 Nrf2 induction does not significantly change Aβ deposition. (A to C) Immunohistochemistry of Aβ in brain sections as shown in a low-magnification image of the hemisphere (A) and high-magnification images of the cerebral cortex (B) and the hippocampus (C) in 11-month-old WT, *App*^{NLGF}, *App*^{NLGF}::*Keap1*$^{FA/FA}$, and *App*^{NLGF}::*Keap1*$^{FA/–}$ mouse brains. (D and E) Quantification of Aβ accumulation. (D) Aβ immunofluorescence in cortex sections of 11-month-old mouse brains. (E) Nine to eleven cortex images per mouse were analyzed, and the percentage of Aβ-positive area in each mouse cortex was calculated ($n = 3$). The percentages of Aβ-positive areas of tissue are represented. (F and G) Aβ content in the brain. Soluble Aβ(1-40) (F) and Aβ(1-42) (G) in the cerebral cortex and the hippocampus (Hippo) of four *App*^{NLGF} and six *App*^{NLGF}::*Keap1*$^{FA/FA}$ 11-month-old mouse brains are shown. Scale bars: 1 mm (A), 200 μm (B), 500 μm (C), and 100 μm (D). The results are presented as means ± the SD. Statistical analyses were performed using the Mann-Whitney U test (E) or ANOVA, followed by the Fisher LSD *post hoc* test (F and G).

in Japanese horseradish, has been reported to mildly activate Nrf2 signaling (54). As we sought to identify a mild Nrf2 inducer that could be administered safely long-term to mice through a nonstressful route, we decided to test the ability of 6-MSITC to preserve the cognitive functions of *App*^{NLGF} mice.

We administered 6-MSITC orally in drinking water during the period from 1 month of age to 11 months of age (Fig. 10A). As we expected, 6-MSITC treatment did not lead to deleterious effects in *App*^{NLGF} mice. Although 6-MSITC is known to be a safe compound without affecting general body conditions or body weight, we examined the body weight changes of the *App*^{NLGF} mice in this study for 16 weeks after the start of administration at 1 month of age. We found that the body weights of the 6-MSITC-treated group of *App*^{NLGF} mice were within a comparable range to those of the water (vehicle)-treated group of mice over the 16 weeks evaluated (Fig. 10B).

We also performed behavior and pathological analyses of these 6-MSITC and vehicle-treated mice, as summarized in Fig. 10A. In very good agreement with the analyses shown in Fig. 2, vehicle-treated *App*^{NLGF} mice displayed impaired escape latency in the PAT compared to vehicle-treated WT mice. Of note, 6-MSITC-treated *App*^{NLGF} mice displayed significant recovery of this impaired escape latency (Fig. 10C). In contrast, the administration of 6-MSITC to WT mice did not change the latency to escape in the PAT. No obvious change was observed in the OFT, the SNORT, or the Y-maze test between vehicle- and 6-MSITC-treated *App*^{NLGF} mice (data not shown).

We then performed immunofluorescent staining for Aβ and Iba1 employing vehicle- and 6-MSITC-treated *App*^{NLGF} mice at 11 months of age. Long-term treatment with 6-MSITC decreased the number of Iba1-positive microglia associated with each amyloid plaque in the *App*^{NLGF} mouse cerebral cortex (Fig. 10D and E). The number of amyloid plaque-associated Iba1-positive microglia per mm^2 of tissue was not significantly reduced in the cortices of 6-MSITC-treated *App*^{NLGF} mice compared to vehicle-treated *App*^{NLGF} mice (Fig. 10F). These results support the notion that long-term treatment with mild chemical Nrf2 inducers can exert partially similar anti-AD activity to that observed by genetic *Keap1* knockdown and Nrf2 induction.

To examine whether 6-MSITC has the ability to activate Nrf2 signaling in the brain, we examined the expression levels of the *Nqo1* gene after 6-MSITC treatment. Since long-term treatment of 6-MSITC to *App*^{NLGF} mice tended to mildly increase *Nqo1* gene expression (Fig. 10G), we used acute Nrf2 induction conditions for this purpose. Intraperitoneal administration of high-dose 6-MSITC (50 mg/kg [body weight]) to WT mice increased *Nqo1* mRNA expression in the cerebral cortex (Fig. 10H), indicating that 6-MSITC can activate Nrf2 signaling in the mouse brain. Taken together, these results support our hypothesis that long-term treatment with mild Nrf2 inducers prevents the onset of cognitive impairment in AD model mice.

Plasmalogen phosphatidylethanolamines in the *App*^{NLGF} mouse brain. It has been reported that plasmalogen phosphatidylethanolamine (PlsPE) levels decrease in the brain and serum of both AD patients and model animals (55–57). PlsPE is a unique class of glycerophospholipid containing a fatty alcohol with a vinyl-ether bond at the *sn*-1 position and a fatty acid at the *sn*-2 position (Fig. 11A). Polyunsaturated fatty acids (PUFAs) are enriched at the *sn*-2 position (58). To verify whether PlsPE acts as a new biomarker for AD and to determine the relationship of PlsPE with Nrf2 in AD pathology, we considered whether the AD mouse model with genetic Keap1 induction would be an optimal system. Therefore, we assessed PlsPE levels in *App*^{NLGF} mice by means of MALDI-MSI analysis.

We first conducted LC-MS analysis and identified nine PlsPE compounds in WT and *App*^{NLGF} mouse brains; this group of PlsPE contained 18:1, 20:4, and 22:6 fatty acids (Fig. 11B). Notably, PlsPE d18:0/22:6 levels were significantly decreased ($P < 0.001$), and PlsPE d18:0/18:1 and d16:0/22:6 levels were mildly decreased ($P = 0.071$ and 0.086, respectively) in *App*^{NLGF} mouse brains compared to WT mouse brains.

To confirm this finding in light of the distributions in the mouse brain, we performed MALDI-MSI analysis with coronal sections from two distinct sites of WT mouse brains, i.e., 1.0 mm anterior and 1.8 mm posterior to the bregma. We focused on three PlsPE compounds, d18:0/22:6, d18:0/18:1, and d16:0/22:6, which were downregulated in *App*^{NLGF} mice compared to WT mice in whole-brain LC-MS analysis (Fig. 11B). We found that the expression profiles of these three PlsPEs were distinct and unique. PlsPE

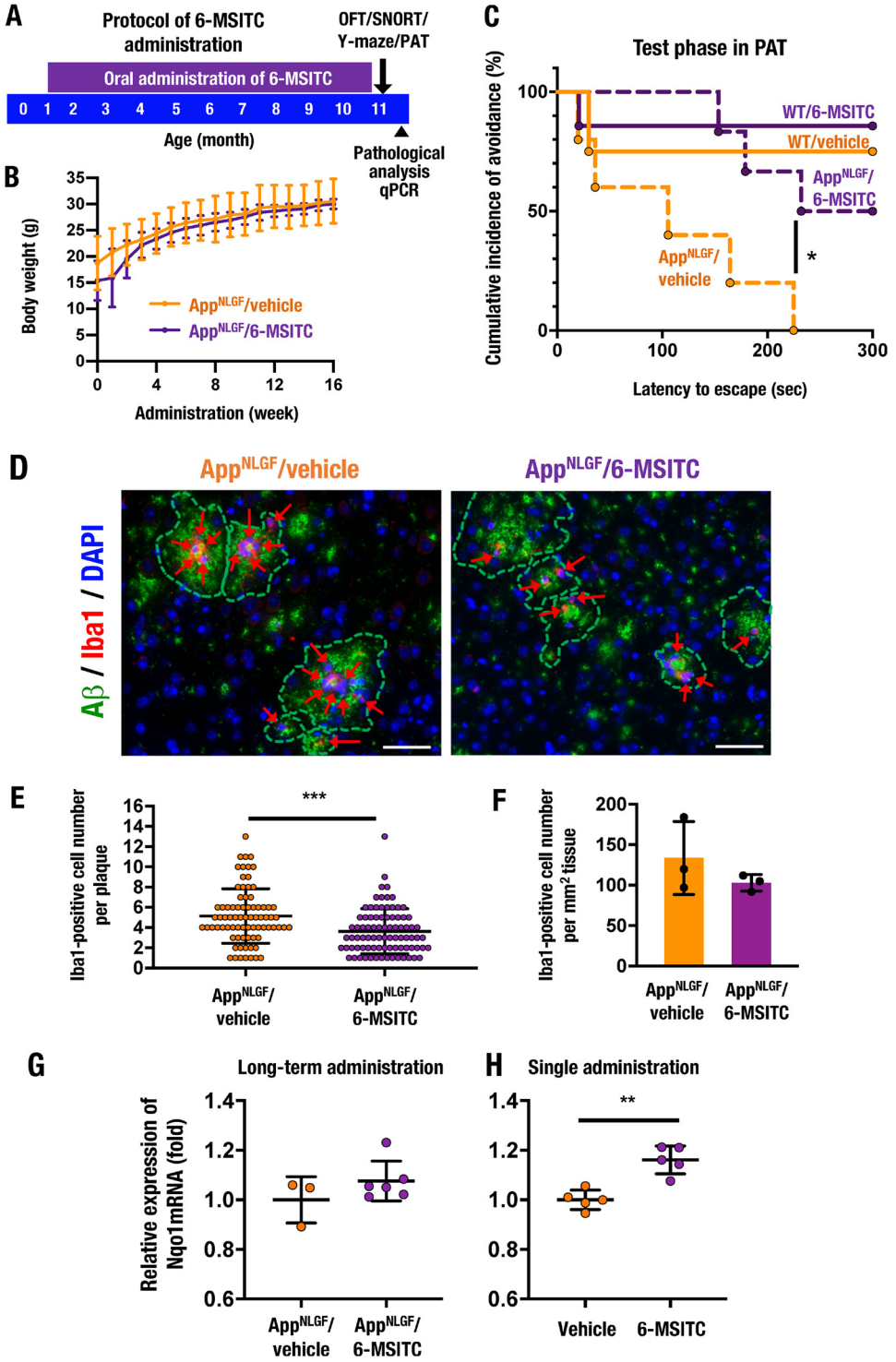

FIG 10 The Nrf2-inducing natural compound 6-MSITC improves cognitive impairment in *App*^{NLGF} mice. (A) A schematic of the protocol for long-term 6-MSITC administration. Vehicle (water) or 6-MSITC was administered to male WT and *App*^{NLGF} mice from 1 month of age to 11 months of age through drinking water. Behavior tests, including the OFT, the SNORT, the Y-maze test, and the PAT, were performed at 11 months of age, followed by pathological analysis and quantitative PCR (qPCR). (B) Time course analysis of body weight in *App*^{NLGF} mice for 16 weeks during long-term administration of vehicle or 6-MSITC. *App*^{NLGF}/vehicle ($n = 8$) and *App*^{NLGF}/6-MSITC ($n = 9$) mice were analyzed. (C) Results of the PAT in 11-month-old male WT/vehicle ($n = 4$), WT/6-MITC ($n = 7$), *App*^{NLGF}/vehicle ($n = 10$), and *App*^{NLGF}/6-MSITC ($n = 10$) mice. The cumulative incidence of avoidance during the test phase is presented. (D) Immunofluorescence staining for Aβ (green) and Iba1 (red) in the cerebral cortices of *App*^{NLGF} mice. ARrows indicate Iba1-positive cells around amyloid plaques. Scale bars, 50 μm. (E) The number of Iba1-positive cells in each amyloid plaque. A total of 78 plaques in the cortices from three *App*^{NLGF}/vehicle mice and

(Continued on next page)

d18:0/22:6 and d16:0/22:6 were both distributed in the cortex, the striatum, the hippocampus, and the center region of the thalamus, whereas PlsPE d18:0/18:1 was highly expressed in the fornix and the thalamus (Fig. 11C and D).

We also compared the levels of these PlsPEs between *App*^{NLGF} and *App*^{NLGF}::*Keap1*$^{FA/FA}$ mice. The levels of PlsPE d16:0/22:6 and d18:0/22:6 were decreased in the hippocampi, thalami, and hypothalami of *App*^{NLGF} mice compared to WT mice; in addition, PlsPE d18:0/18:1 levels were also decreased in the thalami of *App*^{NLGF} mice (Fig. 11E, top and middle panels, arrows). Importantly, the decreases in these PlsPEs were mitigated in *App*^{NLGF}::*Keap1*$^{FA/FA}$ mice (bottom panels, arrows). These data indicate that PlsPE seems to be a useful biomarker for predicting AD conditions and may also be available for evaluating the improvement of AD by Nrf2 inducers.

DISCUSSION

In this study, we addressed the question of how Nrf2 activation prevents the progression of the AD phenotype utilizing AD model mice crossed with *Keap1* knockdown mice. Although several preceding reports have implied an Nrf2 contribution to reducing AD phenotypes, these studies heavily depended on loss-of-function analyses relying on the use of Nrf2 knockout mice (36–39). In contrast, we found in this study that genetic Nrf2 induction by *Keap1* gene knockdown in mice provokes the induction of glutathione synthesis and the repression of inflammatory cytokine gene expression. As summarized in Fig. 12, these changes in gene expression profiles bring about the suppression of amyloid deposition-induced oxidative stress, inflammation, and reactive astrocytosis in *App*^{NLGF} model mouse brains. Existing lines of evidence further support the idea that Nrf2 induction ameliorates the impaired cognitive functions in *App*^{NLGF} mice. In addition to these gene-modified mouse studies, in this study, we also provide evidence that mild, long-term pharmacological induction of Nrf2 by 6-MSITC is able to suppress AD-like pathology in model mice. Based on these findings, we propose that the activation of Nrf2 signaling prevents cognitive impairment in AD.

Whereas the antioxidant system operating in the central nervous system remains to be clarified, Nrf2 has been reported to play critical roles in the regulation of GSH metabolism genes in the brain (7). It has been demonstrated that Nrf2 is strongly induced in astrocytes and microglia but poorly activated in neurons (24, 44, 59). Nrf2 elevates the expression levels of glutathione synthesis-related genes, including the gene for glutamate-cysteine ligase, and enhances the synthesis of GSH in astrocytes (26). Importantly, GSH produced in astrocytes is transported from astrocytes to neurons and exerts beneficial effects in protecting neurons from oxidative damage (24, 60). In this study, we demonstrated that Nrf2 enhanced GSH levels by MALDI-MSI analysis. The elevation of GSH will play important roles in the protection of neurons against various stresses in the *App*^{NLGF} mouse brain.

We believe that GSH-mediated suppression of oxidative stress in the brain is a promising strategy for the prevention and/or early intervention of AD (61). In this regard, however, it has been reported that supplements intended to repress oxidative stresses do not improve the symptoms of AD patients (62–64). In this study, since Nrf2 suppressed both inflammation and oxidative stress in the AD mouse brain, we also focused on inflammation. Importantly, immunoglobulins and complement factors have been reported to be deposited around amyloid plaques in AD patient brains (65). We

FIG 10 Legend (Continued)
85 plaques in the cortices of three *App*^{NLGF}/6-MSITC mice were counted. (F) Amyloid plaque-associated Iba1-positive cell number per tissue area in the cerebral cortex. Ten images per mouse were counted, and the average of numbers in each mouse was calculated in three each of the *App*^{NLGF}/vehicle and *App*^{NLGF}/6-MSITC mice. (G) Expression levels of *Nqo1* mRNA after long-term oral 6-MSITC administration. The cerebral cortices of 11-month-old male *App*^{NLGF}/vehicle ($n = 3$) and *App*^{NLGF}/6-MSITC ($n = 6$) mice were analyzed. (H) Expression levels of *Nqo1* mRNA in the cerebral cortex of 5-week-old male WT mice 12 h after single administration of vehicle or 6-MSITC (50 mg/kg [body weight], intraperitoneally, $n = 5$ each). *Nqo1* expression was normalized to *Actb* expression, and the levels in vehicle-treated mice were set to 1. The results are presented as means ± the SD (B, E to H) or as a Kaplan-Meier curve (C). Statistical analyses were performed using repeated-measures ANOVA (B), the log rank test (C), or the Student *t* test (E to H). *, $P < 0.05$; **, $P < 0.01$; ***, $P < 0.001$.

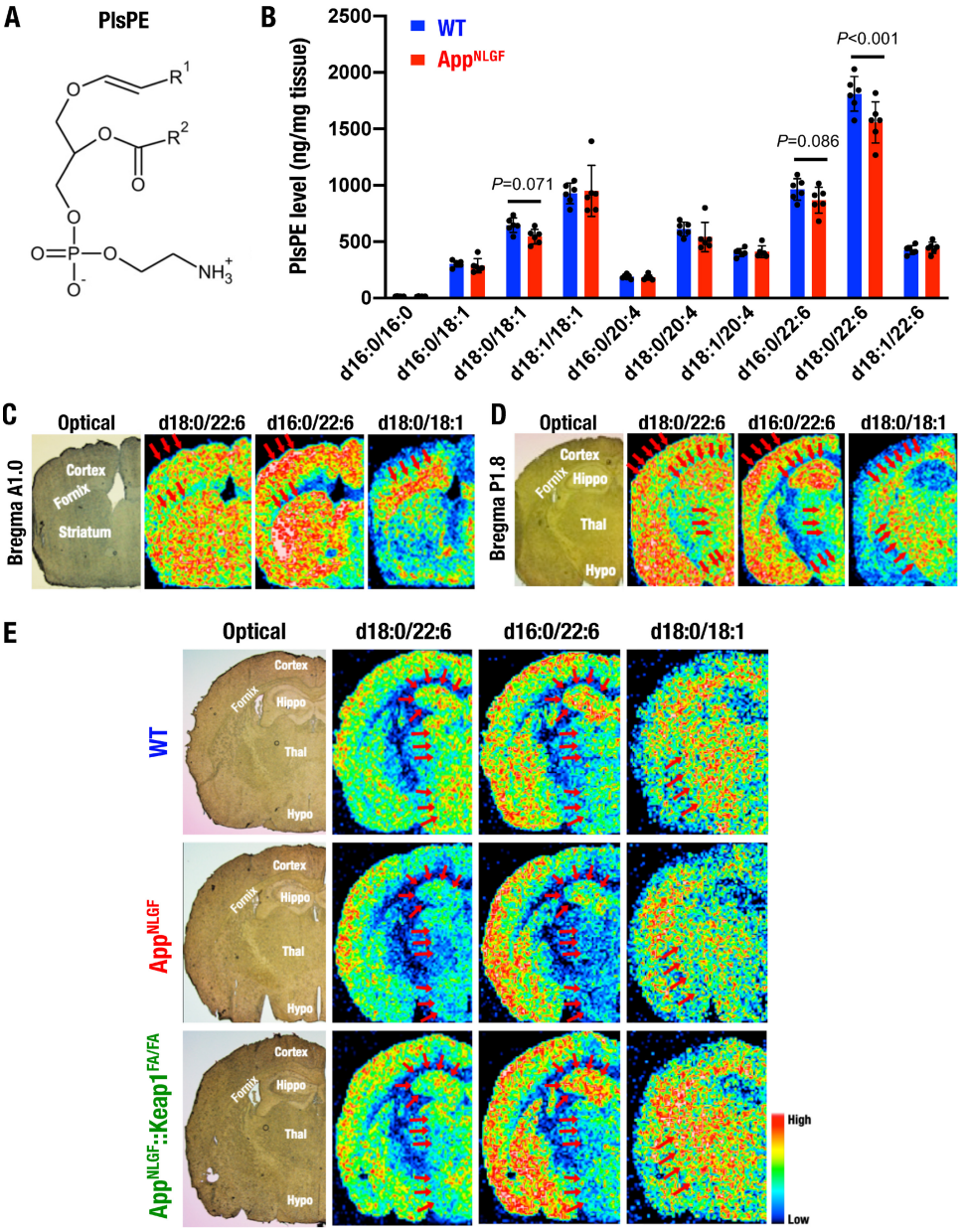

FIG 11 PlsPE as an AD marker in the *App*^{NLGF} mouse brain. (A) Chemical structure of PlsPE containing a fatty alcohol with a vinyl-ether bond at the *sn*-1 position (R^1) and a fatty acid at the *sn*-2 position (R^2). (B) LC-MS analysis of PlsPE in the brains of 8-month-old female WT and *App*^{NLGF} mice (both $n = 6$). The results are presented as means ± the SD. Statistical analyses were performed using ANOVA, followed by the Fisher LSD *post hoc* test. (C to E) MALDI-MSI analyses of PlsPE in the brains of 8-month-old female WT mice (C and D) and 11-month-old male WT, *App*^{NLGF}, and *App*^{NLGF}::*Keap1*$^{FA/FA}$ mice (E). Coronal sections at 1.0 mm anterior (A1.0) (C) and 1.8 mm posterior (P1.8) (D and E) to the bregma were analyzed as special references for the distributions of PlsPEs containing d18:0/22:6, d16:0/22:6, and d18:0/18:1. Experiments were performed at least three times with three mouse brains, and the results were fairly reproducible. Hippo, hippocampus; Thal, thalamus; Hypo, hypothalamus.

also found that Nrf2 inhibited DAM marker expressions in *App*^{NLGF} mouse brain, indicating that Nrf2 suppresses the transition of homeostatic microglia to DAM. It has been reported that TREM2 is expressed in DAM and needed for activation of microglia (48), and *Trem2* depletion decrease Iba1-positive cells and improves pathological changes in AD model mouse brain (66). These observations suggest that the suppression of inflammation is important for controlling the pathogenesis of AD (67, 68). In contrast, anti-inflammatory drugs failed to improve AD symptoms in a previous clinical study (64), and the surveillance in AD patients demonstrated that the loss-of-function

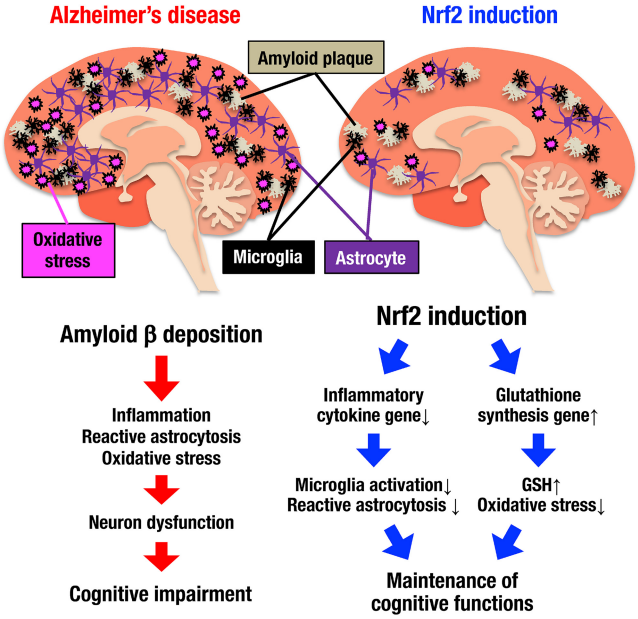

FIG 12 Nrf2 contributes to the maintenance of cognitive functions in AD. Amyloid β deposition (white threads) in the *App*^{NLGF} mouse brain induces inflammation (microglia; black cells), reactive astrocytosis (violet cells), and oxidative stress (pink bombs) and induces the development of neuron dysfunction and cognitive impairment. In contrast, when Nrf2 is induced in the *App*^{NLGF} mouse brain, the expression levels of inflammatory cytokine genes are reduced, and the expression levels of glutathione synthesis-related genes are increased. The number of microglia is decreased, and reactive astrocytosis and oxidative stress are suppressed, while amyloid β deposition remains constant. Nrf2 suppresses inflammation, reactive astrocytosis and oxidative stress in the *App*^{NLGF} mouse brain and contributes to the maintenance of cognitive functions in AD.

TREM2 variant R47H increases the risk of AD (69, 70). Nonetheless, Nrf2 inducers are expected to exert beneficial effects by suppressing the onset and development of AD by simultaneously suppressing oxidative stress and inflammation in the brain.

It has been reported that *App*^{NLGF} mice display amyloid depositions but lack tauopathy or neurofibrillary tangles in the brain (29). Importantly, the PAT analysis in the present study revealed the presence of significant cognitive impairment in *App*^{NLGF} mice. Consistent with this observation, analyses of the other AD mouse models, including Tg2576, APP23, APP/PS1, and 3×Tg-AD mice, also showed the presence of cognitive impairment (71). In this regard, it is interesting to note that AD profiles differ from model to model. For instance, neurofibrillary tangles (NFTs) are observed in 3×Tg-AD mouse brains (72), but NFTs are not observed in the brains of Tg2576, APP/PS1, APP23, or *App*^{NLGF} mice (29, 73–75). Both genetic and pharmacological induction of Nrf2 improved the abnormalities of *App*^{NLGF} mice in the PAT, supporting our belief that the induction of Nrf2 prevents cognitive impairment in the early stage of neurocognitive disorders.

In this study, we found through MALDI-MSI analyses that PUFA-containing PlsPEs are decreased in the hippocampus and the thalamus of the *App*^{NLGF} mouse brain, but genetic Nrf2 induction rescued the suppression of PUFA-containing PlsPEs in the mouse brain. Although the physiological significance of PlsPE changes has not been fully clarified, we posit that PlsPEs may play important roles in the biological membrane, including the maintenance of curved lipid membrane structures, specialized membrane microdomains, and ether-linked glycosylphosphatidylinositols. As it has been reported that the double bond in PUFA contributes to decreasing reactive oxygen species levels (76), the PUFA-containing PlsPEs may contribute to the protection of an AD brain against oxidative stress in collaboration with GSH. While PlsPEs are under evaluation as serum biomarkers of AD in humans (56, 57), our present findings further suggest that PlsPEs may act as useful antioxidants in the AD brain.

In this study, we employed 6-MSITC via a stress-free administration route expecting a mild therapeutic efficacy, as we planned to treat *App*^{NLGF} mice for a long period of time. We found that 6-MSITC improved the pathogenic conditions of *App*^{NLGF} mice in several aspects. Consistent with this finding, it has been reported that 6-MSITC protects neuronal functions in Parkinson's disease model mice (77) and improves memory functions in A$\beta_{1\text{-}42}$ injection-induced cognitive impairment model mice (78). In addition to 6-MSITC, the Nrf2-inducing chemical CDDO-methyl-amide and DMF have been shown to improve cognitive function in other AD model mice (38, 79). These wide-ranging observations provide evidence that Nrf2 inducers are useful drugs for the suppression of AD onset and development.

In conclusion, this study demonstrates that Nrf2 induction improves the antioxidative functions in the brain and ameliorates pathological neuroinflammation in *App*^{NLGF} model mice. This study further provides important lines of evidence supporting the notion that Nrf2 activation suppresses the onset and/or progression of AD, indicating that the Keap1-Nrf2 system is a promising target for the development of drugs for neurocognitive disorders, including AD.

MATERIALS AND METHODS

Animals. *App*^{NLGF}, *Keap1*$^{+/-}$, and *Keap1*$^{FA/FA}$ mice were previously described (29, 42, 80, 81), and these mice were backcrossed to the C57BL/6J strain for at least 10 generations. For pathological and behavioral experiments, we exploited Nrf2-inducing natural compound 6-MSITC (Abcam). 6-MSITC was dissolved in water (0.4 mg/ml) and orally administered *ad libitum* in drinking water to *App*^{NLGF} mice and C57BL/6J strain WT mice for 10 months. To evaluate the expression of the Nrf2 target *Nqo1* gene, 6-MSITC was intraperitoneally administered at 15 mg/kg (body weight), and the brain was collected 12 h after administration. All of the animal experiments were approved by the Animal Committee at Tohoku University.

RNA isolation and real-time quantitative PCR. Total RNA was extracted from the cerebral cortex and the hippocampus with Sepasol-RNA I Super G reagent (Nacalai Tesque). Extracted RNA was used for reverse transcription with ReverTra Ace (Toyobo) according to the manufacturer's instructions. The resulting templates were used for qPCR with Thunderbird qPCR Mix (Toyobo). The primer sets used are listed in Table S1 in the supplemental material. Relative RNA equivalents were obtained by normalization with the expression of *Actb* (encoding β-actin) mRNA levels.

Immunostaining. Immunostaining was performed using mouse monoclonal anti-Aβ (1:300, clone 82E1; IBL), anti-GFAP (clone GA5, 1:300; Chemicon), rabbit polyclonal anti-Iba1 (1:300; Wako), anti-8-OHdG (1:200; Bioss), anti-Tuj1 (1:2,000, ab18207; Abcam) and goat polyclonal anti-NQO1 (1:200, ab2346; Abcam). Secondary antibodies conjugated with horseradish peroxidase, alkaline phosphatase or a fluorescent marker were utilized and visualized according to standard protocols (24). A TUNEL assay for detecting cell death was performed with an *in situ* apoptosis detection kit (TaKaRa). Rat mammary tissue included in the kit was used as a positive control for TUNEL.

The Aβ-positive and GFAP-positive areas were quantified by thresholding the fluorescence intensity in these fluorescent images using ImageJ software. The amyloid plaque-associated Iba-positive cells were manually counted in each Aβ-stained area in the Iba1- and Aβ-double-staining images.

OFT. Mice were videotaped in an open-field test system (O'Hara & Co., Ltd.) to evaluate locomotor, anxiety-like, and exploratory behaviors. A chamber with an open top box (width 50 cm by height 50 cm by depth 30 cm) made of gray acrylic that had photobeam sensors placed 5 cm above the bottom was used to detect vertical activities. Mice were placed in the same chamber for 10 min again to assess habituation behavior in the chamber after 24 h. The behavior of mice in the chamber was monitored for 10 min and recorded by a charge-coupled device camera mounted above the chamber. Videos were analyzed with TimeOFCR4 software (O'Hara & Co., Ltd.). Increased time spent in the central area has been shown to be an index of lower anxiety. The OFT was conducted at 3, 4, 6, 8, 9, and 11 months of age.

PAT. The PAT is a behavioral task assessing learning and memory of aversive spatial information using electric shocks (82). A step-through chamber was prepared consisting of an illuminated acrylic transparent compartment (width 15 cm by height 8.5 cm by depth 25 cm) and a black opaque acrylic chamber (width 25 cm by height 25 cm by depth 25 cm). Two compartments were connected with a hole (5 cm by 5 cm) and a guillotine door. The chamber was placed in a sound-attenuated chamber (width 40 cm by height 60 cm by depth 55 cm; Muromachi Co.), which had a movable and bright-adjustable LED light. The behavior of mice in the chamber was monitored and recorded by a camera mounted above the illuminated compartment.

First, mice were allowed to acclimate to the chamber for 2 min, during which time mice could freely explore the chamber. In the training phase, a mouse was placed in the illuminated chamber with a closed door. The guillotine door was opened 30 s after exposure. A scrambled foot shock (0.35 mA, 2 s) was delivered 3 s after the four paws of the mouse completely entered the dark compartment (LE10026; Panlab). The mouse was moved into a waiting cage 30 s after the foot shock. After 24 h, the mouse was exposed to the chamber again. The latency to enter the dark chamber was calculated in the retention phase.

MALDI-MSI. Mouse brain samples were frozen in liquid nitrogen and dissected for cryosectioning at 8-μm thickness using a cryostat (CM 3050S; Leica Microsystems). Sections were thaw mounted on indium-tin oxide slides (100 Ω/square; Matsunami Co.). For detection of GSH, NEM (Tokyo Chemical Industry) was used to generate GSH-NEM. NEM was dissolved in 15% methanol solution at 100 mmol/liter, and the solution was splayed by using a Mr. Hobby Procon Boy FWA Platinum 0.2 double-action apparatus (GSI Creos). After spraying with NEM solution, specimens were incubated for 60 min at room temperature, after which α-cyano-4-hydroxycinnamic acid (CHCA; Sigma-Aldrich) was applied to the specimens as a matrix at a thickness of 1.5 μm using an iMLayer (Shimadzu).

MALDI-MSI analysis was performed with iMScope (Shimadzu). MS/MS spectra were acquired with 100 laser shots per data point in positive-ion mode. The laser was irradiated at a 25-μm diameter and a 70-μm spatial interval of each data point. Regions of the tissue samples exposed to laser irradiation were determined by light microscopic observations. Metabolites were identified by the MS/MS spectrum using chemical standards. The data were processed using Imaging MS solution v1.30 analysis software (Shimadzu).

For PlsPE detection, CHCA was applied to 0.7-μm-thick specimens, and MS spectra were acquired by 100 laser shots per data point in positive-ion mode. The diameter of laser irradiation was 25 μm, and the spatial interval of each data point was 70 μm.

LC-MS. Frozen mouse brains were dissected for cryosectioning at 8-μm thickness (approximately 0.3 mg) using a cryostat. Sections were placed in 2-ml plastic tubes, and 500 μl of internal standard (sulfide d18:1/17:0, 100 nmol/liter in methanol containing 0.1% formic acid) was added. Samples were vigorously mixed for 15 sec and homogenized in an ultrasonic bath for 10 min and then centrifuged at 16,000 $\times$ *g* for 20 min. The supernatant was then injected into the UPLC-MS/MS system. UHPLC-MS/MS analysis was performed on an Acquity Ultra Performance LC I-class system equipped with a binary solvent manager, a sample manager, and a column heater (Waters) interfaced with a Waters Xevo TQ-S MS/MS system equipped with electrospray ionization operated in positive-ion mode (83).

MS/MS was performed using multiple reaction monitoring mode; the transitions of the precursor ion to the product ion, cone voltage (V), and collision energy (eV) are listed in Table S2 in the supplemental material. The capillary voltage was 2.5 kV, and the cone voltage was 100 V. The source offset and temperature were set at 50 V and 150°C, respectively, with a cone gas flow rate of 150 liters/h. The desolvation temperature was set to 500°C, and the desolvation gas flow, collision gas flow, and nebulization gas flow were set to 1,000 liters/h, 0.15 ml/min, and 7.00 $\times$ 10^5 Pa, respectively. Both the cone and the nebulization gases were nitrogen. LC separation was performed using a reversed-phase column (Acquity UPLC BEH C8; 150 mm by 2.1 mm [inner diameter], 1.7-μm particle size; Waters Corp.) with a gradient elution of solvent A (5 mmol/liter ammonium formate in water, pH 4) and solvent B (5 mmol/liter ammonium formate in 95% acetonitrile, pH 4) at 0.4 ml/min. The initial condition was set to 40% solvent B and maintained for 1 min, and solvent B was increased linearly to 80% over 4 min. The gradient continued from 80 to 95% solvent B in the next 3 min and from 95 to 100% in 2 min. Subsequently, solvent B was immediately set to 100% and maintained for 8 min. Finally, the mobile phase was returned to the initiated conditions and maintained for 7 min until the end of the run (84). The oven temperature was 45°C. Data were collected using MassLynx v4.1 software (Waters) and analyzed using Traverse MS v1.2.7 software (Reifycs).

Aβ ELISA. Cerebral cortices and hippocampi were added with 5$\times$ volume Tris-buffered saline (pH 7.4) with protease inhibitor cocktail Complete (Roche) and sonicated with a Sonifier 250 sonicator (Branson) for 45 s (85), followed by centrifugation at 17,400 $\times$ *g* for 60 min. To quantitate the levels of Aβ(1-40) and Aβ(1-42), the supernatant was analyzed by a Human β Amyloid(1-40)ELISA kit Wako II and a Human β Amyloid(1-42) ELISA kit Wako, High Sensitive (Fujifilm Wako Pure Chemical) according to the manufacturer's instructions.

Statistical analyses. Data are presented as the means $\pm$ the standard deviations (SD) or as a Kaplan-Meier survival curve. Statistical analyses were performed using Student's *t* test and the Mann-Whitney U test for two groups. Analyses of variance (ANOVA), followed by the Fisher least-significant-difference (LSD) *post hoc* test and the Kruskal-Wallis test, were performed for multiple comparisons. A log rank test was performed for the Kaplan-Meier survival curve.

SUPPLEMENTAL MATERIAL

Supplemental material for this article is available online only.

SUPPLEMENTAL FILE 1, PDF file, 0.1 MB.

SUPPLEMENTAL FILE 2, PDF file, 0.1 MB.

SUPPLEMENTAL FILE 3, PDF file, 0.03 MB.

SUPPLEMENTAL FILE 4, PDF file, 0.02 MB.

ACKNOWLEDGMENTS

We thank Nao Ota (Tohoku University) and the Tohoku University Graduate School of Medicine Biomedical Research Core for technical support.

This research was supported by the Platform Project for Supporting Drug Discovery and Life Science Research (Basis for Supporting Innovative Drug Discovery and Life Science Research [BINDS]) from the Japan Agency for Medical Research and Development (AMED; grant JP19am0101001 [M.Y.]), by the Tohoku Medical Megabank Project

from the Ministry of Education, Culture, Sports, Science, and Technology (MEXT), by AMED (JP18km0105001 and JP18km0105002 [M.Y.]), by Grants-in-Aid for Scientific Research from the Japan Society for the Promotion of Science (JSPS; grants 24249015 and 19H01019 [M.Y.], grants 17K01837 and 16KK0195 [A.U.], and grant 19K07361 [D.M.]), by the Takeda Science Foundation (M.Y.), and by the Naito Foundation (M.Y.).

REFERENCES

1. Ferri CP, Prince M, Brayne C, Brodaty H, Fratiglioni L, Ganguli M, Hall K, Hasegawa K, Hendrie H, Huang Y, Jorm A, Mathers C, Menezes PR, Rimmer E, Scazufca M, Alzheimer's Disease International. 2005. Global prevalence of dementia: a Delphi consensus study. Lancet 366:2112–2117. https://doi.org/10.1016/S0140-6736(05)67889-0.
2. Ballard C, Gauthier S, Corbett A, Brayne C, Aarsland D, Jones E. 2011. Alzheimer's disease. Lancet 377:1019–1031. https://doi.org/10.1016/S0140-6736(10)61349-9.
3. Chauhan V, Chauhan A. 2006. Oxidative stress in Alzheimer's disease. Pathophysiology 13:195–208. https://doi.org/10.1016/j.pathophys.2006.05.004.
4. Henstridge CM, Hyman BT, Spires-Jones TL. 2019. Beyond the neuron-cellular interactions early in Alzheimer disease pathogenesis. Nat Rev Neurosci 20:94–108. https://doi.org/10.1038/s41583-018-0113-1.
5. Saito T, Saido TC. 2018. Neuroinflammation in mouse models of Alzheimer's disease. Clin Exp Neuroimmunol 9:211–218. https://doi.org/10.1111/cen3.12475.
6. Uruno A, Yagishita Y, Yamamoto M. 2015. The Keap1-Nrf2 system and diabetes mellitus. Arch Biochem Biophys 566:76–84. https://doi.org/10.1016/j.abb.2014.12.012.
7. Itoh K, Chiba T, Takahashi S, Ishii T, Igarashi K, Katoh Y, Oyake T, Hayashi N, Satoh K, Hatayama I, Yamamoto M, Nabeshima Y. 1997. An Nrf2/small Maf heterodimer mediates the induction of phase II detoxifying enzyme genes through antioxidant response elements. Biochem Biophys Res Commun 236:313–322. https://doi.org/10.1006/bbrc.1997.6943.
8. Itoh K, Wakabayashi N, Katoh Y, Ishii T, Igarashi K, Engel JD, Yamamoto M. 1999. Keap1 represses nuclear activation of antioxidant responsive elements by Nrf2 through binding to the amino-terminal Neh2 domain. Genes Dev 13:76–86. https://doi.org/10.1101/gad.13.1.76.
9. Itoh K, Igarashi K, Hayashi N, Nishizawa M, Yamamoto M. 1995. Cloning and characterization of a novel erythroid cell-derived CNC family transcription factor heterodimerizing with the small Maf family proteins. Mol Cell Biol 15:4184–4193. https://doi.org/10.1128/mcb.15.8.4184.
10. Sykiotis GP, Bohmann D. 2010. Stress-activated cap'n'collar transcription factors in aging and human disease. Sci Signal 3:re3. https://doi.org/10.1126/scisignal.3112re3.
11. Kobayashi A, Kang MI, Watai Y, Tong KI, Shibata T, Uchida K, Yamamoto M. 2006. Oxidative and electrophilic stresses activate Nrf2 through inhibition of ubiquitination activity of Keap1. Mol Cell Biol 26:221–229. https://doi.org/10.1128/MCB.26.1.221-229.2006.
12. Tong KI, Padmanabhan B, Kobayashi A, Shang C, Hirotsu Y, Yokoyama S, Yamamoto M. 2007. Different electrostatic potentials define ETGE and DLG motifs as hinge and latch in oxidative stress response. Mol Cell Biol 27:7511–7521. https://doi.org/10.1128/MCB.00753-07.
13. Fukutomi T, Takagi K, Mizushima T, Ohuchi N, Yamamoto M. 2014. Kinetic, thermodynamic, and structural characterizations of the association between Nrf2-DLGex degron and Keap1. Mol Cell Biol 34:832–846. https://doi.org/10.1128/MCB.01191-13.
14. Takaya K, Suzuki T, Motohashi H, Onodera K, Satomi S, Kensler TW, Yamamoto M. 2012. Validation of the multiple sensor mechanism of the Keap1-Nrf2 system. Free Radic Biol Med 53:817–827. https://doi.org/10.1016/j.freeradbiomed.2012.06.023.
15. Saito R, Suzuki T, Hiramoto K, Asami S, Naganuma E, Suda H, Iso T, Yamamoto H, Morita M, Baird L, Furusawa Y, Negishi T, Ichinose M, Yamamoto M. 2016. Characterizations of three major cysteine sensors of Keap1 in stress response. Mol Cell Biol 36:271–284. https://doi.org/10.1128/MCB.00868-15.
16. Yamazaki H, Katsuoka F, Motohashi H, Engel JD, Yamamoto M. 2012. Embryonic lethality and fetal liver apoptosis in mice lacking all three small Maf proteins. Mol Cell Biol 32:808–816. https://doi.org/10.1128/MCB.06543-11.
17. Yamamoto M, Kensler TW, Motohashi H. 2018. The KEAP1-NRF2 system: a thiol-based sensor-effector apparatus for maintaining redox homeostasis. Physiol Rev 98:1169–1203. https://doi.org/10.1152/physrev.00023.2017.
18. Ishii T, Itoh K, Takahashi S, Sato H, Yanagawa T, Katoh Y, Bannai S, Yamamoto M. 2000. Transcription factor Nrf2 coordinately regulates a group of oxidative stress-inducible genes in macrophages. J Biol Chem 275:16023–16029. https://doi.org/10.1074/jbc.275.21.16023.
19. Kobayashi EH, Suzuki T, Funayama R, Nagashima T, Hayashi M, Sekine H, Tanaka N, Moriguchi T, Motohashi H, Nakayama K, Yamamoto M. 2016. Nrf2 suppresses macrophage inflammatory response by blocking proinflammatory cytokine transcription. Nat Commun 7:11624. https://doi.org/10.1038/ncomms11624.
20. Itoh K, Mochizuki M, Ishii Y, Ishii T, Shibata T, Kawamoto Y, Kelly V, Sekizawa K, Uchida K, Yamamoto M. 2004. Transcription factor Nrf2 regulates inflammation by mediating the effect of 15-deoxy-$\Delta^{12,14}$-prostaglandin J_2. Mol Cell Biol 24:36–45. https://doi.org/10.1128/mcb.24.1.36-45.2004.
21. Yagishita Y, Uruno A, Chartoumpekis DV, Kensler TW, Yamamoto M. 2019. Nrf2 represses the onset of type 1 diabetes in non-obese diabetic mice. J Endocrinol https://doi.org/10.1530/JOE-18-0355.
22. Higashi C, Kawaji A, Tsuda N, Hayashi M, Saito R, Yagishita Y, Suzuki T, Uruno A, Nakamura M, Nakao K, Furusako S, Yamamoto M. 2017. The novel Nrf2 inducer TFM-735 ameliorates experimental autoimmune encephalomyelitis in mice. Eur J Pharmacol 802:76–84. https://doi.org/10.1016/j.ejphar.2017.02.044.
23. Suzuki T, Murakami S, Biswal SS, Sakaguchi S, Harigae H, Yamamoto M, Motohashi H. 2017. Systemic activation of NRF2 alleviates lethal autoimmune inflammation in scurfy mice. Mol Cell Biol 37:e00063-17.
24. Yagishita Y, Uruno A, Fukutomi T, Saito R, Saigusa D, Pi J, Fukamizu A, Sugiyama F, Takahashi S, Yamamoto M. 2017. Nrf2 improves leptin and insulin resistance provoked by hypothalamic oxidative stress. Cell Rep 18:2030–2044. https://doi.org/10.1016/j.celrep.2017.01.064.
25. Muramatsu H, Katsuoka F, Toide K, Shimizu Y, Furusako S, Yamamoto M. 2013. Nrf2 deficiency leads to behavioral, neurochemical, and transcriptional changes in mice. Genes Cells 18:899–908. https://doi.org/10.1111/gtc.12083.
26. Kraft AD, Johnson DA, Johnson JA. 2004. Nuclear factor E2-related factor 2-dependent antioxidant response element activation by *tert*-butylhydroquinone and sulforaphane occurring preferentially in astrocytes conditions neurons against oxidative insult. J Neurosci 24:1101–1112. https://doi.org/10.1523/JNEUROSCI.3817-03.2004.
27. Yoshida H, Mimura J, Imaizumi T, Matsumiya T, Ishikawa A, Metoki N, Tanji K, Ota K, Hayakari R, Kosaka K, Itoh K, Satoh K. 2011. Edaravone and carnosic acid synergistically enhance the expression of nerve growth factor in human astrocytes under hypoxia/reoxygenation. Neurosci Res 69:291–298. https://doi.org/10.1016/j.neures.2010.12.016.
28. Yang L, Calingasan NY, Thomas B, Chaturvedi RK, Kiaei M, Wille EJ, Liby KT, Williams C, Royce D, Risingsong R, Musiek ES, Morrow JD, Sporn M, Beal MF. 2009. Neuroprotective effects of the triterpenoid, CDDO methyl amide, a potent inducer of Nrf2-mediated transcription. PLoS One 4:e5757. https://doi.org/10.1371/journal.pone.0005757.
29. Saito T, Matsuba Y, Mihira N, Takano J, Nilsson P, Itohara S, Iwata N, Saido TC. 2014. Single *App* knock-in mouse models of Alzheimer's disease. Nat Neurosci 17:661–663. https://doi.org/10.1038/nn.3697.
30. Youssef P, Chami B, Lim J, Middleton T, Sutherland GT, Witting PK. 2018. Evidence supporting oxidative stress in a moderately affected area of the brain in Alzheimer's disease. Sci Rep 8:11553. https://doi.org/10.1038/s41598-018-29770-3.
31. Castillo E, Leon J, Mazzei G, Abolhassani N, Haruyama N, Saito T, Saido T, Hokama M, Iwaki T, Ohara T, Ninomiya T, Kiyohara Y, Sakumi K, LaFerla FM, Nakabeppu Y. 2017. Comparative profiling of cortical gene expression in Alzheimer's disease patients and mouse models demonstrates a link between amyloidosis and neuroinflammation. Sci Rep 7:17762. https://doi.org/10.1038/s41598-017-17999-3.

32. Ansari MA, Scheff SW. 2010. Oxidative stress in the progression of Alzheimer disease in the frontal cortex. J Neuropathol Exp Neurol 69:155–167. https://doi.org/10.1097/NEN.0b013e3181cb5af4.
33. Karelson E, Bogdanovic N, Garlind A, Winblad B, Zilmer K, Kullisaar T, Vihalemm T, Kairane C, Zilmer M. 2001. The cerebrocortical areas in normal brain aging and in Alzheimer's disease: noticeable differences in the lipid peroxidation level and in antioxidant defense. Neurochem Res 26:353–361. https://doi.org/10.1023/a:1010942929678.
34. Griffin WS, Stanley LC, Ling C, White L, MacLeod V, Perrot LJ, White CL, Araoz C. 1989. Brain interleukin 1 and S-100 immunoreactivity are elevated in Down syndrome and Alzheimer disease. Proc Natl Acad Sci U S A 86:7611–7615. https://doi.org/10.1073/pnas.86.19.7611.
35. Rogers J, Luber-Narod J, Styren SD, Civin WH. 1988. Expression of immune system-associated antigens by cells of the human central nervous system: relationship to the pathology of Alzheimer's disease. Neurobiol Aging 9:339–349. https://doi.org/10.1016/s0197-4580(88)80079-4.
36. Rojo AI, Pajares M, Rada P, Nuñez A, Nevado-Holgado AJ, Killik R, Van Leuven F, Ribe E, Lovestone S, Yamamoto M, Cuadrado A. 2017. NRF2 deficiency replicates transcriptomic changes in Alzheimer's patients and worsens APP and TAU pathology. Redox Biol 13:444–451. https://doi.org/10.1016/j.redox.2017.07.006.
37. Branca C, Ferreira E, Nguyen TV, Doyle K, Caccamo A, Oddo S. 2017. Genetic reduction of Nrf2 exacerbates cognitive deficits in a mouse model of Alzheimer's disease. Hum Mol Genet 26:4823–4835. https://doi.org/10.1093/hmg/ddx361.
38. Rojo AI, Pajares M, García-Yagüe AJ, Buendia I, Van Leuven F, Yamamoto M, López MG, Cuadrado A. 2018. Deficiency in the transcription factor NRF2 worsens inflammatory parameters in a mouse model with combined tauopathy and amyloidopathy. Redox Biol 18:173–180. https://doi.org/10.1016/j.redox.2018.07.006.
39. Joshi G, Gan KA, Johnson DA, Johnson JA. 2015. Increased Alzheimer's disease-like pathology in the APP/PS1ΔE9 mouse model lacking Nrf2 through modulation of autophagy. Neurobiol Aging 36:664–679. https://doi.org/10.1016/j.neurobiolaging.2014.09.004.
40. Kanninen K, Malm TM, Jyrkkänen HK, Goldsteins G, Keksa-Goldsteine V, Tanila H, Yamamoto M, Ylä-Herttuala S, Levonen AL, Koistinaho J. 2008. Nuclear factor erythroid 2-related factor 2 protects against beta amyloid. Mol Cell Neurosci 39:302–313. https://doi.org/10.1016/j.mcn.2008.07.010.
41. Kanninen K, Heikkinen R, Malm T, Rolova T, Kuhmonen S, Leinonen H, Ylä-Herttuala S, Tanila H, Levonen AL, Koistinaho M, Koistinaho J. 2009. Intrahippocampal injection of a lentiviral vector expressing Nrf2 improves spatial learning in a mouse model of Alzheimer's disease. Proc Natl Acad Sci U S A 106:16505–16510. https://doi.org/10.1073/pnas.0908397106.
42. Taguchi K, Maher JM, Suzuki T, Kawatani Y, Motohashi H, Yamamoto M. 2010. Genetic analysis of cytoprotective functions supported by graded expression of Keap1. Mol Cell Biol 30:3016–3026. https://doi.org/10.1128/MCB.01591-09.
43. Habas A, Hahn J, Wang X, Margeta M. 2013. Neuronal activity regulates astrocytic Nrf2 signaling. Proc Natl Acad Sci U S A 110:18291–18296. https://doi.org/10.1073/pnas.1208764110.
44. Bell KF, Al-Mubarak B, Martel MA, McKay S, Wheelan N, Hasel P, Márkus NM, Baxter P, Deighton RF, Serio A, Bilican B, Chowdhry S, Meakin PJ, Ashford ML, Wyllie DJ, Scannevin RH, Chandran S, Hayes JD, Hardingham GE. 2015. Neuronal development is promoted by weakened intrinsic antioxidant defences due to epigenetic repression of Nrf2. Nat Commun 6:7066. https://doi.org/10.1038/ncomms8066.
45. Lastres-Becker I, García-Yagüe AJ, Scannevin RH, Casarejos MJ, Kügler S, Rábano A, Cuadrado A. 2016. Repurposing the NRF2 activator dimethyl fumarate as therapy against synucleinopathy in Parkinson's disease. Antioxid Redox Signal 25:61–77. https://doi.org/10.1089/ars.2015.6549.
46. Suganuma H, Fahey JW, Bryan KE, Healy ZR, Talalay P. 2011. Stimulation of phagocytosis by sulforaphane. Biochem Biophys Res Commun 405:146–151. https://doi.org/10.1016/j.bbrc.2011.01.025.
47. Stratoulias V, Venero JL, Tremblay M, Joseph B. 2019. Microglial subtypes: diversity within the microglial community. EMBO J 38:e101997. https://doi.org/10.15252/embj.2019101997.
48. Keren-Shaul H, Spinrad A, Weiner A, Matcovitch-Natan O, Dvir-Szternfeld R, Ulland TK, David E, Baruch K, Lara-Astaiso D, Toth B, Itzkovitz S, Colonna M, Schwartz M, Amit I. 2017. A unique microglia type associated with restricting development of Alzheimer's disease. Cell 169:1276–1290.e1217. https://doi.org/10.1016/j.cell.2017.05.018.
49. Deczkowska A, Keren-Shaul H, Weiner A, Colonna M, Schwartz M, Amit I. 2018. Disease-associated microglia: a universal immune sensor of neurodegeneration. Cell 173:1073–1081. https://doi.org/10.1016/j.cell.2018.05.003.
50. Krasemann S, Madore C, Cialic R, Baufeld C, Calcagno N, El Fatimy R, Beckers L, O'Loughlin E, Xu Y, Fanek Z, Greco DJ, Smith ST, Tweet G, Humulock Z, Zrzavy T, Conde-Sanroman P, Gacias M, Weng Z, Chen H, Tjon E, Mazaheri F, Hartmann K, Madi A, Ulrich JD, Glatzel M, Worthmann A, Heeren J, Budnik B, Lemere C, Ikezu T, Heppner FL, Litvak V, Holtzman DM, Lassmann H, Weiner HL, Ochando J, Haass C, Butovsky O. 2017. The TREM2-APOE pathway drives the transcriptional phenotype of dysfunctional microglia in neurodegenerative diseases. Immunity 47:566–581.e569. https://doi.org/10.1016/j.immuni.2017.08.008.
51. Rossi R, Milzani A, Dalle-Donne I, Giustarini D, Lusini L, Colombo R, Di Simplicio P. 2002. Blood glutathione disulfide: *in vivo* factor or *in vitro* artifact? Clin Chem 48:742–753.
52. Giustarini D, Tsikas D, Colombo G, Milzani A, Dalle-Donne I, Fanti P, Rossi R. 2016. Pitfalls in the analysis of the physiological antioxidant glutathione (GSH) and its disulfide (GSSG) in biological samples: an elephant in the room. J Chromatogr B Analyt Technol Biomed Life Sci 1019:21–28. https://doi.org/10.1016/j.jchromb.2016.02.015.
53. Moore T, Le A, Niemi AK, Kwan T, Cusmano-Ozog K, Enns GM, Cowan TM. 2013. A new LC-MS/MS method for the clinical determination of reduced and oxidized glutathione from whole blood. J Chromatogr B Analyt Technol Biomed Life Sci 929:51–55. https://doi.org/10.1016/j.jchromb.2013.04.004.
54. Hou DX, Korenori Y, Tanigawa S, Yamada-Kato T, Nagai M, He X, He J. 2011. Dynamics of Nrf2 and Keap1 in ARE-mediated NQO1 expression by wasabi 6-(methylsulfinyl)hexyl isothiocyanate. J Agric Food Chem 59:11975–11982. https://doi.org/10.1021/jf2032439.
55. Han X, Holtzman DM, McKeel DW. 2001. Plasmalogen deficiency in early Alzheimer's disease subjects and in animal models: molecular characterization using electrospray ionization mass spectrometry. J Neurochem 77:1168–1180. https://doi.org/10.1046/j.1471-4159.2001.00332.x.
56. Wood PL, Locke VA, Herling P, Passaro A, Vigna GB, Volpato S, Valacchi G, Cervellati C, Zuliani G. 2016. Targeted lipidomics distinguishes patient subgroups in mild cognitive impairment (MCI) and late onset Alzheimer's disease (LOAD). BBA Clin 5:25–28. https://doi.org/10.1016/j.bbacli.2015.11.004.
57. Goodenowe DB, Cook LL, Liu J, Lu Y, Jayasinghe DA, Ahiahonu PW, Heath D, Yamazaki Y, Flax J, Krenitsky KF, Sparks DL, Lerner A, Friedland RP, Kudo T, Kamino K, Morihara T, Takeda M, Wood PL. 2007. Peripheral ethanolamine plasmalogen deficiency: a logical causative factor in Alzheimer's disease and dementia. J Lipid Res 48:2485–2498. https://doi.org/10.1194/jlr.P700023-JLR200.
58. Braverman NE, Moser AB. 2012. Functions of plasmalogen lipids in health and disease. Biochim Biophys Acta 1822:1442–1452. https://doi.org/10.1016/j.bbadis.2012.05.008.
59. Soriano FX, Léveillé F, Papadia S, Higgins LG, Varley J, Baxter P, Hayes JD, Hardingham GE. 2008. Induction of sulfiredoxin expression and reduction of peroxiredoxin hyperoxidation by the neuroprotective Nrf2 activator 3H-1,2-dithiole-3-thione. J Neurochem 107:533–543. https://doi.org/10.1111/j.1471-4159.2008.05648.x.
60. Dringen R, Pfeiffer B, Hamprecht B. 1999. Synthesis of the antioxidant glutathione in neurons: supply by astrocytes of CysGly as precursor for neuronal glutathione. J Neurosci 19:562–569. https://doi.org/10.1523/JNEUROSCI.19-02-00562.1999.
61. Pocernich CB, Butterfield DA. 2012. Elevation of glutathione as a therapeutic strategy in Alzheimer disease. Biochim Biophys Acta 1822:625–630. https://doi.org/10.1016/j.bbadis.2011.10.003.
62. Persson T, Popescu BO, Cedazo-Minguez A. 2014. Oxidative stress in Alzheimer's disease: why did antioxidant therapy fail? Oxid Med Cell Longev 2014:427318. https://doi.org/10.1155/2014/427318.
63. Kim GH, Kim JE, Rhie SJ, Yoon S. 2015. The role of oxidative stress in neurodegenerative diseases. Exp Neurobiol 24:325–340. https://doi.org/10.5607/en.2015.24.4.325.
64. Nichols MR, St-Pierre MK, Wendeln AC, Makoni NJ, Gouwens LK, Garrad EC, Sohrabi M, Neher JJ, Tremblay ME, Combs CK. 2019. Inflammatory mechanisms in neurodegeneration. J Neurochem 149:562–581. https://doi.org/10.1111/jnc.14674.
65. Eikelenboom P, Stam FC. 1982. Immunoglobulins and complement factors in senile plaques: an immunoperoxidase study. Acta Neuropathol 57:239–242. https://doi.org/10.1007/bf00685397.
66. Jay TR, Miller CM, Cheng PJ, Graham LC, Bemiller S, Broihier ML, Xu G, Margevicius D, Karlo JC, Sousa GL, Cotleur AC, Butovsky O, Bekris L,

Staugaitis SM, Leverenz JB, Pimplikar SW, Landreth GE, Howell GR, Ransohoff RM, Lamb BT. 2015. TREM2 deficiency eliminates TREM2+ inflammatory macrophages and ameliorates pathology in Alzheimer's disease mouse models. J Exp Med 212:287–295. https://doi.org/10.1084/jem.20142322.
67. Arranz AM, De Strooper B. 2019. The role of astroglia in Alzheimer's disease: pathophysiology and clinical implications. Lancet Neurol 18:406–414. https://doi.org/10.1016/S1474-4422(18)30490-3.
68. Edwards FA. 2019. A unifying hypothesis for Alzheimer's disease: from plaques to neurodegeneration. Trends Neurosci 42:310–322. https://doi.org/10.1016/j.tins.2019.03.003.
69. Guerreiro R, Alzheimer Genetic Analysis Group, Wojtas A, Bras J, Carrasquillo M, Rogaeva E, Majounie E, Cruchaga C, Sassi C, Kauwe JS, Younkin S, Hazrati L, Collinge J, Pocock J, Lashley T, Williams J, Lambert JC, Amouyel P, Goate A, Rademakers R, Morgan K, Powell J, St George-Hyslop P, Singleton A, Hardy J. 2013. TREM2 variants in Alzheimer's disease. N Engl J Med 368:117–127. https://doi.org/10.1056/NEJMoa1211851.
70. Jonsson T, Stefansson H, Steinberg S, Jonsdottir I, Jonsson PV, Snaedal J, Bjornsson S, Huttenlocher J, Levey AI, Lah JJ, Rujescu D, Hampel H, Giegling I, Andreassen OA, Engedal K, Ulstein I, Djurovic S, Ibrahim-Verbaas C, Hofman A, Ikram MA, van Duijn CM, Thorsteinsdottir U, Kong A, Stefansson K. 2013. Variant of TREM2 associated with the risk of Alzheimer's disease. N Engl J Med 368:107–116. https://doi.org/10.1056/NEJMoa1211103.
71. Webster SJ, Bachstetter AD, Nelson PT, Schmitt FA, Van Eldik LJ. 2014. Using mice to model Alzheimer's dementia: an overview of the clinical disease and the preclinical behavioral changes in 10 mouse models. Front Genet 5:88. https://doi.org/10.3389/fgene.2014.00088.
72. Oddo S, Caccamo A, Shepherd JD, Murphy MP, Golde TE, Kayed R, Metherate R, Mattson MP, Akbari Y, LaFerla FM. 2003. Triple-transgenic model of Alzheimer's disease with plaques and tangles: intracellular Aβ and synaptic dysfunction. Neuron 39:409–421. https://doi.org/10.1016/s0896-6273(03)00434-3.
73. Radde R, Bolmont T, Kaeser SA, Coomaraswamy J, Lindau D, Stoltze L, Calhoun ME, Jäggi F, Wolburg H, Gengler S, Haass C, Ghetti B, Czech C, Hölscher C, Mathews PM, Jucker M. 2006. Aβ42-driven cerebral amyloidosis in transgenic mice reveals early and robust pathology. EMBO Rep 7:940–946. https://doi.org/10.1038/sj.embor.7400784.
74. Sturchler-Pierrat C, Abramowski D, Duke M, Wiederhold KH, Mistl C, Rothacher S, Ledermann B, Bürki K, Frey P, Paganetti PA, Waridel C, Calhoun ME, Jucker M, Probst A, Staufenbiel M, Sommer B. 1997. Two amyloid precursor protein transgenic mouse models with Alzheimer disease-like pathology. Proc Natl Acad Sci U S A 94:13287–13292. https://doi.org/10.1073/pnas.94.24.13287.
75. Hsiao K, Chapman P, Nilsen S, Eckman C, Harigaya Y, Younkin S, Yang F, Cole G. 1996. Correlative memory deficits, Aβ elevation, and amyloid plaques in transgenic mice. Science 274:99–102. https://doi.org/10.1126/science.274.5284.99.
76. Markesbery WR. 1997. Oxidative stress hypothesis in Alzheimer's disease. Free Radic Biol Med 23:134–147. https://doi.org/10.1016/s0891-5849(96)00629-6.
77. Morroni F, Sita G, Tarozzi A, Cantelli-Forti G, Hrelia P. 2014. Neuroprotection by 6-(methylsulfinyl)hexyl isothiocyanate in a 6-hydroxydopamine mouse model of Parkinson's disease. Brain Res 1589:93–104. https://doi.org/10.1016/j.brainres.2014.09.033.
78. Morroni F, Sita G, Graziosi A, Turrini E, Fimognari C, Tarozzi A, Hrelia P. 2018. Protective effects of 6-(methylsulfinyl)hexyl isothiocyanate on Aβ. Int J Mol Sci 19:E2083.
79. Dumont M, Wille E, Calingasan NY, Tampellini D, Williams C, Gouras GK, Liby K, Sporn M, Nathan C, Flint Beal M, Lin MT. 2009. Triterpenoid CDDO-methylamide improves memory and decreases amyloid plaques in a transgenic mouse model of Alzheimer's disease. J Neurochem 109:502–512. https://doi.org/10.1111/j.1471-4159.2009.05970.x.
80. Wakabayashi N, Itoh K, Wakabayashi J, Motohashi H, Noda S, Takahashi S, Imakado S, Kotsuji T, Otsuka F, Roop DR, Harada T, Engel JD, Yamamoto M. 2003. Keap1-null mutation leads to postnatal lethality due to constitutive Nrf2 activation. Nat Genet 35:238–245. https://doi.org/10.1038/ng1248.
81. Okawa H, Motohashi H, Kobayashi A, Aburatani H, Kensler TW, Yamamoto M. 2006. Hepatocyte-specific deletion of the *keap1* gene activates Nrf2 and confers potent resistance against acute drug toxicity. Biochem Biophys Res Commun 339:79–88. https://doi.org/10.1016/j.bbrc.2005.10.185.
82. Ader R. 1973. Effects of early experiences on shock-and illness-induced passive avoidance behaviors. Dev Psychobiol 6:547–555. https://doi.org/10.1002/dev.420060611.
83. Saigusa D, Okudaira M, Wang J, Kano K, Kurano M, Uranbileg B, Ikeda H, Yatomi Y, Motohashi H, Aoki J. 2014. Simultaneous quantification of sphingolipids in small quantities of liver by LC-MS/MS. Mass Spectrom (Tokyo) 3:S0046. https://doi.org/10.5702/massspectrometry.S0046.
84. Sato K, Saigusa D, Saito R, Fujioka A, Nakagawa Y, Nishiguchi KM, Kokubun T, Motoike IN, Maruyama K, Omodaka K, Shiga Y, Uruno A, Koshiba S, Yamamoto M, Nakazawa T. 2018. Metabolomic changes in the mouse retina after optic nerve injury. Sci Rep 8:11930. https://doi.org/10.1038/s41598-018-30464-z.
85. Wang J, Dickson DW, Trojanowski JQ, Lee VM. 1999. The levels of soluble versus insoluble brain Aβ distinguish Alzheimer's disease from normal and pathologic aging. Exp Neurol 158:328–337. https://doi.org/10.1006/exnr.1999.7085.